# AN INTEGRATED FRINGE COUNTING AND INTERPOLATION LASER HETERODYNE INTERFEROMETER FOR MICRO-ROBOT POSITION MEASUREMENT

by
**Paul Gilles Charette**

A thesis submitted to
the Faculty of Graduate Studies and Research
in partial fulfilment of the requirements for the degree of
Master of Engineering

Biorobotics Laboratory
Department of Biomedical Engineering
and
Department of Electrical Engineering
McGill University
Montréal, Québec, Canada
September, 1990

# ABSTRACT

This thesis describes a laser heterodyne interferometer for measuring the displacement of a high performance micro-robot limb. The limb movements must be measured over a range of 10 mm, with a resolution of 1 nm *SD* (standard deviation), in experiments lasting less than 1 second. The maximum displacement speed of the limbs is 2 m/s.

To fulfil the design requirements, the approach taken here is to consider that the full measurement resolution is only needed when the limb is approaching its target at low speed.

The interferometer described in this thesis is capable of high accuracy fringe interpolation measurements over a range of 10 mm, with a resolution of 0.1 nm *SD*, in a bandwidth of 100 kHz, in a 1 second time period. For low resolution measurements when the limb is moving at high speed, the interferometer measures displacements by fringe counting.

Experimental results are presented which demonstrate that the accuracy of the interferometer actually exceeds the high resolution design objective by an order of magnitude. Also, results of experiments which study the effect of noise sources (both inherent to the interferometer and from the environment) on the accuracy of the measurements are presented.

Finally, results of an experiment where the interferometer was used in a practical application to demonstrate its usefulness are presented: the interferometer was used in the closed-loop control of a non-linear micro-actuator.

# RESUME

Cette thèse décrit un interféromètre laser utilisé pour mesurer les déplacements d'un micro-robot à haute performance. La position du micro-robot doit être mesurée avec une précision d'au moins 1 nm (écart type), sur une distance de 10 mm, lors d'expériences durant moins d'une seconde. Le micro-robot peut se déplacer à une vitesse maximale de 2 m/s.

L'hypothèse de base considérée ici est que la pleine précision dans les mesures de la position n'est requise que lorsque le robot s'approche à basse vitesse de son objectif.

L'interféromètre étudié ici est capable de mesurer les déplacements du micro-robot avec une précision de 0.1 nm (écart type) sur une longueur totale de 10 mm, et ce, dans une bande passante de 100 kHz, dans une période de une seconde. Lors des déplacements à hautes vitesses, l'interféromètre mesure la position du micro-robot avec une précision réduite en comptant les franges optiques.

Les résultats expérimentaux présentés dans cette thèse démontrent que la performance de l'interféromètre dépasse l'objectif de précision fixé dans le cadre de ce projet par un facteur 10. Ces résultats étudient également l'effet des sources de bruit (propres à l'interféromètre et provenant de l'environnement) sur la précision des mesures.

Enfin, les résultats d'une expérience utilisant l'interféromètre dans une application pratique sont présentés: l'interféromètre a été utilisé pour controller avec précision les déplacements d'un moteur électro-magnétique, dont la fonction de transfer est non-linéaire.

# ACKNOWLEDGEMENTS

This research project was actually a highly successful collaborative effort between the Biorobotics lab at McGill University and MPB Technologies Inc. of Dorval. In my opinion, the success of this project can be attributed to a large extent to the pooling of expertise with my collaborators from MPB and McGill.

Most of the experimental work was carried out in the Lasers and Electro-Optics laboratories at MPB technologies Inc., thanks to the company's generous contribution in lab space and equipment.

I would first like to thank my supervisor Dr. Ian Hunter, for his help and guidance. The amazing breath of his scientific knowledge, and his enthusiastic and rigorous style of research have had a profound influence on me.

I would like to thank Dr. Morrel Bachynski, president of MPB Technologies Inc. for his support. His company's contribution to this project in equipment, expertise and financial support have been invaluable.

Special thanks to Mr. Colin Brenan of MPB Technologies Inc. for his tutoring in laser physics, his endless patience, and his permanent willingness to help in the many discussions that went into this design.

Special thanks to Mr. Damjan Jocic of MPB Technologies Inc. for his help in designing the high frequency electronics, and to all the Lasers and Electro-Optics group for their assistance.

I would also like to thank Mr. Serge Lafontaine for his technical advice and aid with the computing facilities in the Biorobotics laboratory.

Last but not least, I would like to thank my parents for their encouragement and support, and Manon Beaulieu for her kindness and understanding.

I am very grateful to the Medical Research Council of Canada and the Fonds pour la Formation de Chercheurs et l'Aide à la Recherche (FCAR) for financially supporting this research

# TABLE OF CONTENTS

# LIST OF FIGURES

# LIST OF TABLES

# CHAPTER ONE: INTRODUCTION AND DESIGN RATIONALE

## 1.1 Prologue and Outline

In the past three years, Dr. Ian Hunter and his group have designed, built and tested a high performance medical micro-robot at McGill University (Hunter *et al.*, 1990). This micro-robot, used for single muscle cell manipulation and mechanical testing, is capable of very accurate three dimensional motion at high speed.

Until now, the performance of the micro-robot has been limited by its position transducers which are custom built linear variable differential transformers (LVDT). The LVDTs resolve 10 nm SD (standard deviation) in 1 mm (i.e.: dynamic range of $10^5$) in a DC to 10 kHz bandwidth. This corresponds to a *dynamic range-bandwidth product* of $10^9$ Hz. The micro-robot actuators however have an estimated dynamic range-bandwidth product of $10^{12}$ Hz. Hence a higher performance type of position transducer is required to enable the micro-robot to benefit from the full potential of its actuators.

This thesis demonstrates a laser heterodyne interferometry technique that has a dynamic range-bandwidth product of $10^{12}$ Hz. The laser interferometer described here combines the extended range and speed features of conventional fringe counting techniques with the high accuracy characteristics of high performance interpolation interferometers.

Chapter 1 overviews the fields of micro-robotics and interferometry, and explains the choice of a particular interferometry technique in relation to the design criteria. Chapter 2 explains the details of the design and the choice of components. Chapter 3 analyzes the various error sources and presents experimental results. Chapter 4 lists some possible improvements to the design and projected future expansions.

## 1.2 Overview of Micro-Robotics

The field of micro-robotics is actually the combination of two apparently similar but fairly distinct areas. The first is the science of building microscopic sized machines. It is hoped that such "micro-machines" will someday be capable of elaborate tasks in very small remote areas, such as repair work inside small structures (e.g., human blood vessels).

The second area of micro-robotics is the science of building machines for micro-manipulation, where the machines themselves can be fairly large in comparison to their workspace. Such "micro-manipulators" however are capable of much higher forces and stiffness than the "micro-machines". The micro-robot designed by Dr. Hunter falls into the "micro-manipulator" category. This latter field of micro-robotics is briefly reviewed below.

There is a growing need in science and industry for "micro-manipulators" which are capable of handling very small objects, in such diverse fields as DNA surgery for genetic engineering (object size < 1 μm), to micro-machining for micro-sensor construction (object size < 100 μm).

Microscopic objects have been typically manipulated using linear translation stages stacked in a serial x-y-z configuration to provide three axis motion. Piezoelectric slabs are sometimes inserted in series with the translation stages to produce submicrometer movement.

This type of arrangement is known as a *serial* configuration. While this configuration can attain high accuracy, it has two serious drawbacks. The first is that the translation stages are much too slow for many applications (typically 5 mm/s or less). The second drawback is that each motor in the stack must drive the other stages above it. Consequently, each motor drives a different inertia, and so the mechanical characteristics across axes are different.

These drawbacks have been known and discussed for some time in micro-robotics. For example, in the early sixties, Ellis (1962) proposed various parallel

configurations involving piezoelectric ceramic actuators. Several other micro-robot designs have since been proposed and a few are presented below to give the reader a feeling for the diversity in the field.

More recently, Hollis *et al.* (1990) described a tele "nano-manipulator" where active magnetic levitation is used in a master coupled with a scanning tunnelling microscope slave. Objects are scanned by servo controlling the height of a platinum tip at the end of a PZT tube. The tube is bent in the $x$, $y$ and $z$ directions by biasing its orthogonal outer electrodes. The system is capable of atomic scale force feedback and motion resolution.

Higuchi *et al.* (1990) describe a serial configuration for a four degree of freedom micro-manipulator arm. The arm consists of a 1 degree of freedom rotating joint attached to a three degree of freedom joint. Their system uses friction and inertial forces caused by rapid deformations of micro-piezoelectric elements to produce motion ("inch-worm" drives).

At McGill University, Hunter *et al.* (1990) have designed and tested a high performance parallel configuration micromanipulator. The apparatus is driven closed-loop with force and displacement feedback. Teleoperation is achieved via a human interface macro duplicate of the micromanipulator. This is the system for which the displacement transducer presented in this report has been designed. The specifics of this micro-robot are described briefly in the following section.

## 1.3 Description of High Performance Micro-Robot

The interest in high performance micromanipulators in Dr. Hunter's lab evolved from their experimental requirements for the study of living muscle cells. Currently, muscle is modelled as a lumped or black-box non-linear system for force and stiffness prediction experiments. As muscle is not a homogeneous system however, such models are of limited scientific interest. Rather, it is highly

desirable to move to 3-D mechanical and optical measurements and continuum models aimed at understanding the role of the different force-generating elements within each muscle cell.

For this purpose, a micro-robot having two high performance parallel limbs has been developed in Dr. Hunter's laboratory for the manipulation and mechanical testing of living muscle cells.

Each limb is composed of three orthogonal linear axes attached at an end point platform (apex). Each linear axis is actuated by a piezoelectric slab (displacement range up to 1 μm) mounted on a linear electromagnetic motor (displacement range up to 6 mm). Quartz tube beams emanating from the actuator end points are joined together at one end (apex), forming a stiff and high speed positioning system. The end points of each micro-robot limb move in an overlapping spherical workspace of 1 mm in diameter.

Figure 1-1 shows a schematic diagram of the orientation in space of the two limbs, each with its three orthogonal axes. Figure 1-2 shows a top view of the micro-robot apparatus and associated Michelson and Mach-Zender interferometers used for various muscle experiments. The setup is mounted on an optical table and inclosed in a lead-felt-copper cage for thermal and vibration isolation. Figure 1-3 shows a front view photograph of the micro-robot apparatus on the optical table.

High resolution LVDTs are used on each of the six cascaded actuator assemblies to measure the displacement of the quartz beams. A simple geometric transformation is required to determine the position of the apex, from the measured displacements of the three quartz beams.

As stated in the overview, the performance of the micro-robot is limited by its position transducers. It is estimated that the cascaded actuator assemblies of the micro-robot limbs can move the apex over a range of 6 mm with a resolution of around 0.1 nm (i.e.: $6 \times 10^7$ dynamic range).

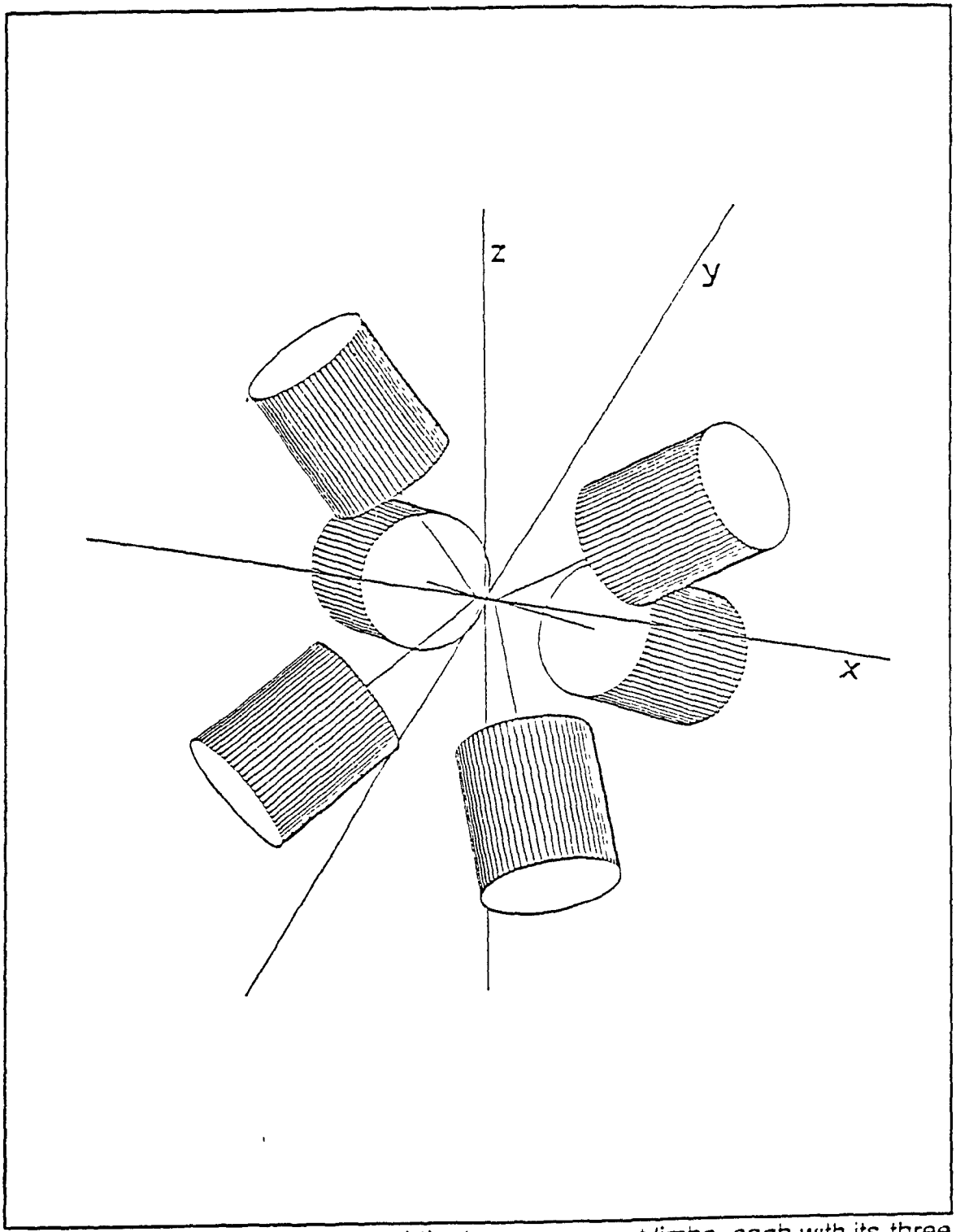


**Figure 1-1.** Schematic diagram of the two micro-robot limbs, each with its three orthogonal linear axes.

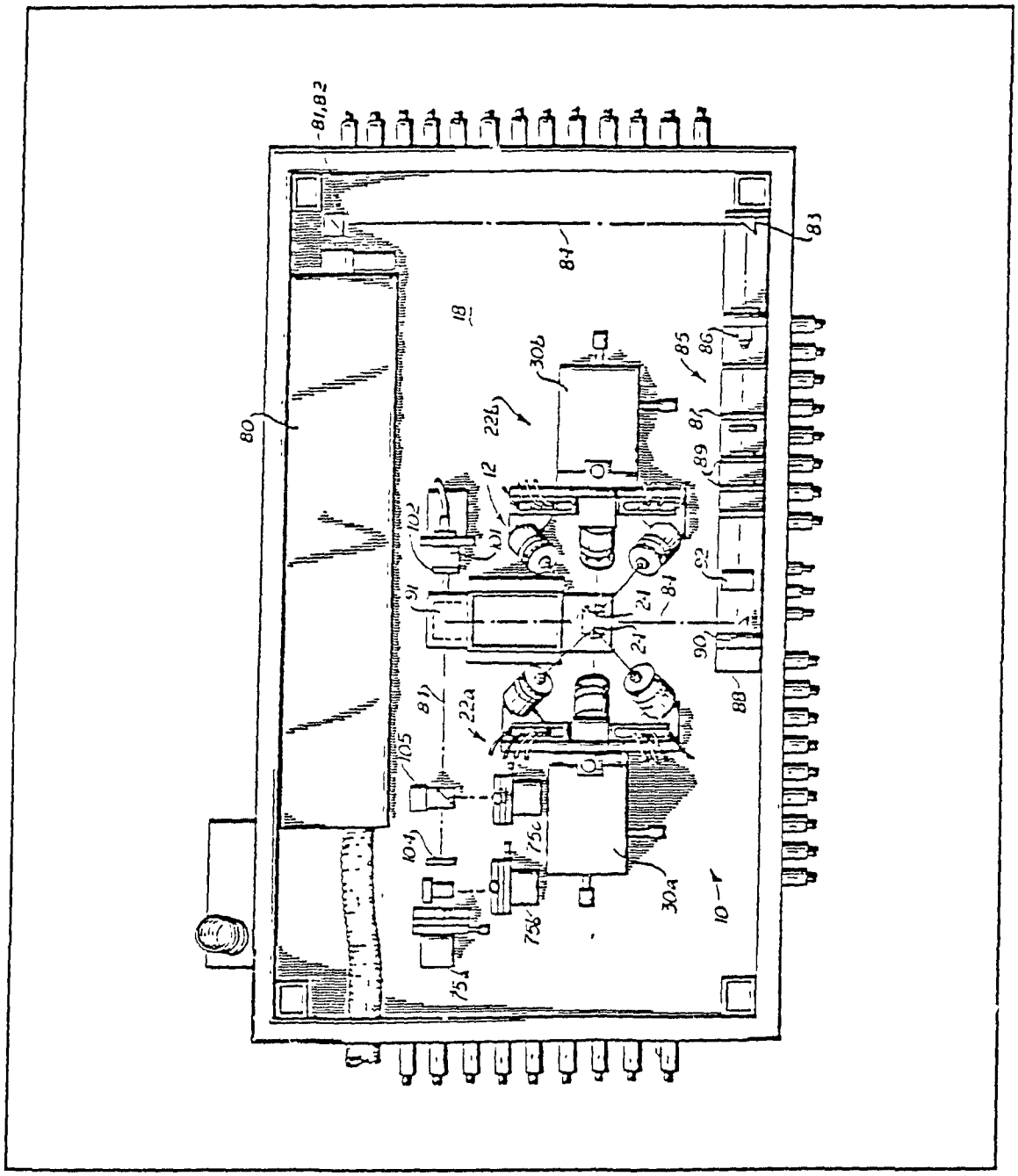


Figure 1-2. Top view schematic diagram of the micro-robot apparatus on the optical table. (Micro-robot limb endpoints: 24, translation stages to initially position the limbs: 30, laser: 80, interferometer optics: 81 to 105, photo-detectors: 75).

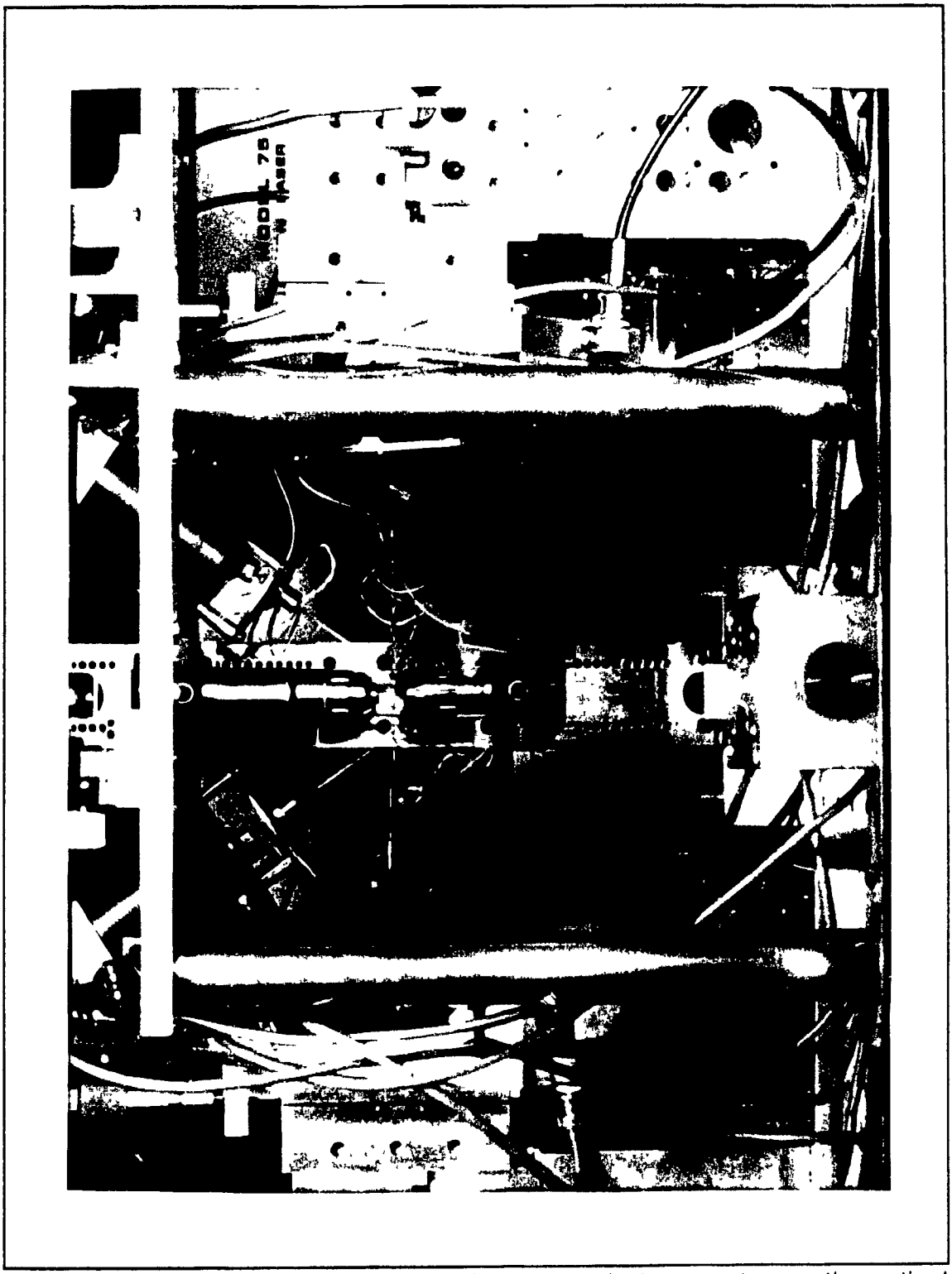

**Figure 1-3.** Front view photograph of the micro-robot apparatus on the optical table.

Furthermore, the actuators are capable of moving the limb end points at a maximum velocity of 2 m/s, at frequencies up to 18 kHz. Hence, the dynamic range-bandwidth product of the actuators is ~ $10^{12}$ Hz.

## 1.4 Design Objective and Choice of Displacement Transducer Technology

The design objective of this research project was to produce a displacement transducer with a dynamic range-bandwidth product equal or superior to that of the micro-robot actuators, over a measurement period of 1 second (the typical experiment duration for muscle cell experiments with the micro-robot).

Under the assumption that the full measurement resolution is needed only when the micro-robot limbs approach their target at low speeds, the transducer was required to meet two extreme specifications:

1) A "high accuracy, low speed" mode with an accuracy of 1 nm *SD* over a range of 10 mm when the micro-robot is approaching its target. In this mode, the maximum allowable bandwidth is 100 kHz.

2) A "low accuracy, high speed" mode with an accuracy of ≈ 150 nm *SD* over a range of 10 mm, when the micro-robot limbs are moving at a maximum velocity of 2 m/s.

Several types of displacement transducers were considered by Dr. Hunter and his associates in the development phases of the micro-robot. The performance of the various devices tested are compared to in Table 1-1.

Note that the values listed in the table for interferometry are ideal, since new techniques which come ever closer to the theoretical limit are constantly emerging. The maximum range for laser interferometry is equal to the coherence length of the source (several kilometres in the case of certain lasers) and the

theoretical limit on resolution is around $10^{-15}$ m•Hz$^{0.5}$ (Wagner *et al.*, 1987). The measurement bandwidth for interferometry is theoretically limited to the oscillation frequency of electric field of the light source, which is in the range of $0.5x10^{15}$ Hz for a Helium-Neon laser for example. Practical considerations for electronic phase demodulation however usually limit the bandwidth to the megahertz range.

Comparing the design objective shown at the bottom of Table 1-1 to the list of the various available techniques, it is apparent that the LVDTs are inadequate and that laser interferometry is the only available displacement transducer technology with both sufficient dynamic range and bandwidth.

| **Transducer Technology** | **Dynamic Range** | **Bandwidth** | **Product** |
|---|---|---|---|
| Potentiometers | $5x10^3$ | 100 Hz | $5x10^8$ Hz |
| Strain Gauge | $10^4$ | 10 kHz | $10^8$ Hz |
| Capacitances Transducers | $10^4$ | 50 kHz | $5x10^8$ Hz |
| Lateral Effect Photo-Diodes | $10^6$ | 10 kHz | $10^{10}$ Hz |
| LVDT | $10^4$ | 10 kHz | $10^8$ Hz |
| Laser Interferometry | $> 10^{12}$ | > 1 MHz | $10^{18}$ Hz |
| DESIGN OBJECTIVE: | $10^7$ | 100 kHz | $10^{12}$ Hz |

**Table 1-1.** List of displacement transducer technologies that could be used for measuring the displacement of the micro-robot limbs.

## 1.5 Overview of Interferometry

The physics of electromagnetic wave interference have been well known for some time. Until a few years ago however, although interferometry was of significant scientific interest, its practical applications were few. With the recent availability of the laser, the use of interferometry has undergone an explosive growth of applications in science and industry (Hariharan, 1987). The applications of laser interferometry range from metrology, vibration analysis, stress and strain analysis and surface micro-profiling, to measurements of the refractive index of gasses, coefficients of thermal expansion and many others material properties.

### 1.5.1 Temporal Coherence

The main advantage of the laser over other available light sources is its long coherence length. The notion of temporal coherence is central to interferometry so it is briefly explained in this section.

To understand coherence, imagine that light is made up of wave trains of finite length, of which a large number pass at random time intervals during the time required to make an observation. The phase of the light is constant over a particular wave train, but the change in phase between wave trains is random.

The average length of a wave train is termed the coherence length $\Delta l$. The time taken by light to travel the coherence length, or equivalently, the average time over which the phase of the light is constant, is called the coherence time $\Delta t$, where,

$$\Delta l = c \bullet \Delta t. \qquad (1.1)$$

From Fourier theory, we know that a light wave with a single frequency (delta function in the frequency domain) must have infinite duration in the time domain (Eykhoff, 1974). Since the wave trains have a finite length $\Delta t$ in the time

domain, it follows that the frequency content of the light of each wave train is not a single value but a spread of frequencies.

It can be shown (Born & Wolf, 1980) that the coherence length $\Delta l$ of a light source is related to its frequency bandwidth $\Delta v$ (spectral linewidth) by the following inequality,

$$\Delta l \bullet \Delta v \geq c / 4\pi, \tag{1.2}$$

where $c$ is the speed of light.

For comparison purposes, the coherence length of different light sources are listed in Table 1-2 (adapted from Gasvik, 1987).

| LIGHT SOURCE | $\Delta l$ |
|---|---|
| Broadband visible light | < 1 μm |
| Discharge lamps | a few mm |
| Isotope lamps ($Hg^{198}$, $Kr^{86}$) | < 1 m |
| Lasers | up to several km |

**Table 1-2.** Light source coherence lengths (Adapted from Gaswick, 1987).

### 1.5.2 Michelson Interferometer

To best explain interferometry, we refer to the basic Michelson interferometer design shown in Figure 1-4. The light emitted by the laser is divided by the beamsplitter *BS* into two equal amplitude wavefronts along the *local oscillator* path $E_{lo}(\omega_{lo}, \phi_{lo})$, and the *signal* path $E_s(\omega_s, \phi_s)$ respectively, where $E$ is the electric field, $\omega$ is the frequency of the light and $\phi$ is the phase.

Both paths are then recombined by the beamsplitter and the resulting interference pattern is measured at a photo-detector. Any displacement of the moving mirror will cause a change in the distance travelled by the light in the signal path, thus changing the interference pattern.

An optional frequency shifter in either arm of the interferometer will cause the interference pattern to oscillate at the difference frequency. This is desirable in certain situations, as explained in Section 1.6.

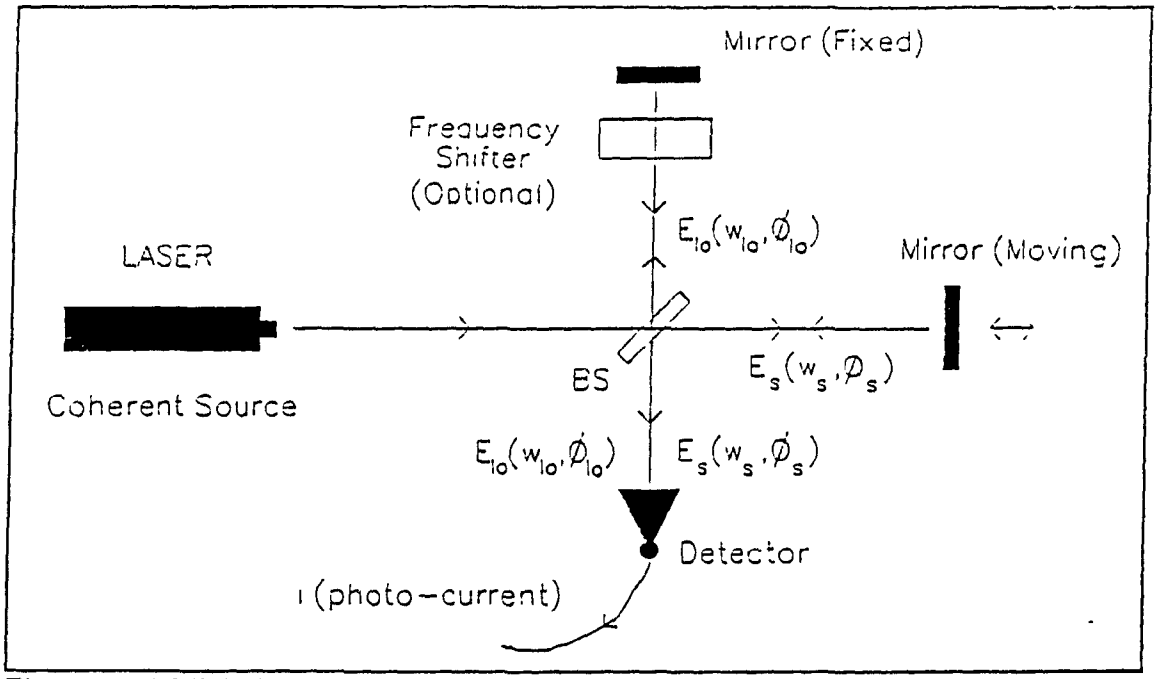


Figure 1-4 Michelson Interferometer.

The objective of interferometry is to infer the change in the moving mirror position from the change in the phase between the interfering wavefronts at the detector. Hence we describe in the equations below the mathematical relationship between the moving mirror displacement *d* and the total electric field at the detector.

The electric fields from the local oscillator and signal paths in the interferometer are formally defined as,

$$E_{lo} = E_{lo}\exp[j(kx_{lo} - \omega_{lo}t)], \quad (1.3)$$

and,

$$E_s = E_s\exp[j(kx_s - \omega_s t)], \quad (1.4)$$

where,

$E_{lo}$ and $E_s$ are the amplitudes of the electric fields,
$x_{lo}$ and $x_s$ are the paths travelled by the waves along each arm,
$k_{lo}$ and $k_s$ are the propagation numbers of the electric fields, and
exp[] denotes the exponential function $e^x$.

The propagation number $k$ is defined as,

$$k = 2\pi/\lambda, \quad (1.5)$$

where $\lambda$ is the wavelength of the source in the medium.

Hence, the phase $\phi$ of each wavefront is specified by,

$$\phi = kx. \quad (1.6)$$

The total electric field $E_{tot}$ resulting from the mixing of the beams from the two paths at the detector is,

$$E_{tot} = E_{lo} + E_s. \quad (1.7)$$

Since the electric field $E$ of light varies at an exceeding high rate (in the range of $10^{15}$ Hz), it is an impractical quantity to detect directly. The irradiance $I$ however can be measured with a wide variety of sensors (photo-cells, bolometers, photographic emulsions, etc.). Assuming both electric fields to be perfectly collinear (Hecht, 1987), the irradiance $I$ can be expressed as,

$$\begin{aligned} I &= \varepsilon_o c\langle E_{TOT}^2 \rangle, \\ &= \varepsilon_o c\{(E_{Io}^2/2) + (E_s^2/2) + E_{Io}E_s\cos(\Delta\omega t + k\Delta x)\}, \\ &= I_{Io} + I_s + 2(I_{Io}I_s)^{1/2}\cos(\Delta\omega t + k\Delta x), \end{aligned} \qquad (1.8)$$

where,

$I_{Io} = \varepsilon_o c E_{Io}^2/2$,
$I_s = \varepsilon_o c E_s^2/2$,
$\Delta\omega = \omega_{Io} - \omega_s$,
$\Delta x = x_{Io} - x_s$ (known as the path length difference),
$\varepsilon_o$ is the permittivity of free space ($8.8542 \times 10^{-12}$ $C^2N^{-1}m^{-2}$),
$c$ is the speed of light,
and <> denotes the time averaged value.

The information carrying term $\cos(\Delta\omega t + k\Delta x)$ is known as the *interference term*. The irradiance $I$ reaches a maximum when $k\Delta x$ is an even multiple of $\pi$, and it reaches a minimum when $k\Delta x$ is an odd multiple of $\pi$.

If we consider that the moving mirror is at the "origin" when its position is such that the path length difference $\Delta x$ is null (i.e.: $x_{Io} = x_s$), then any displacement $d$ from this point can be expressed as,

$$2d = \Delta x. \qquad (1.9)$$

Finally, by substituting Equation 1.9 into Equation 1.8, the desired relation between the mirror displacement $d$ and the total electric field $E_{TOT}$ at the detector (through the irradiance $I$) is expressed by,

$$I = I_{Io} + I_s + 2(I_{Io}I_s)^{1/2}\cos(\Delta\omega t + 2kd) \qquad (1.10)$$

As stated above, the irradiance $I$ can be measured with a variety of devices. In the case of a photo-detector, the output current $i$ is directly proportional to the irradiance $I$ incident onto the detector surface.

This section is concluded by explaining the connection between the coherence length $\Delta l$, explained in Section 1.5.1, and the measure of mirror displacement $d$.

In the derivation of the Equation 1.10 above, total coherence of the two interfering wavefronts was assumed for simplicity in the mathematics. In actual fact however, Equation 1.10 should be written as (Born & Wolf, 1987),

$$I = I_{lo} + I_s + 2(I_{lo}I_s)^{1/2}|\gamma_{slo}(d)|\cos(\Delta\omega t + 2kd) \qquad (1.11)$$

where $\gamma_{slo}(d)$ is the *complex degree of coherence*, and $0 \leq |\gamma_{slo}(d)| \leq 1$.

When the path length difference $\Delta x$ is null, the complex degree of coherence is identically equal to 1. When the path length difference $\Delta x$ is equal to the coherence length $\Delta l$ however, the complex degree of coherence is identically equal to 0, and the interference pattern is not observable.

This can be understood qualitatively by considering that when the path length difference is less than $\Delta l$, there is some degree of overlap at the detector between interfering phase coherent wavefronts originating from the same wave train. The interference pattern visibility deteriorates (i.e.: $\gamma_{slo}(d)$ decreases) as the path length difference increases, or equivalently as the overlap between phase coherent interfering wavefronts decreases.

Hence, the uncertainty on the measurement of the mirror position increases as $d$ increases, and the limit on the range of measurement is the coherence length $\Delta l$.

## 1.6 Survey of Existing Interferometer Designs

There are a large variety of available techniques in the literature for recovering the path length difference *d* from the measured photocurrent *i*. They can be broadly classified into three categories by the particular signal property that is used to encode the information: amplitude, phase, or frequency. The different interferometry techniques differ in terms of resolution, range, bandwidth. Furthermore, they also differ in their respective robustness to hostile environmental conditions and noise.

In this section, an overview is given of the more common interferometry techniques in the literature, including specific results whenever they are stated in the papers. The choice of a particular type of technique for this project is then explained. Note that only interferometry techniques specific to displacement measurement will be considered. Related topics such as absolute distance interferometry, surface profiling or vibration analysis, although very similar in theory of operation, exceed the scope of this report.

### 1.6.1 Amplitude Encoded Information techniques

In the classical Michelson design, there is no frequency shift in either of the interferometer arms (see Figure 1-4, without the frequency shifter), thus $\omega_s = \omega_{lo}$ and $\Delta\omega = 0$. This technique is termed *homodyne interferometry*, where Equation (1.10) reduces to,

$$I = I_{lo} + I_s + 2(I_{lo}I_s)^{1/2}\cos(2kd). \qquad \textbf{(1.12)}$$

Hence, in homodyne interferometry, the amplitude of the photocurrent *i* is directly proportional to *cos(2kd)*.

### 1.6.1.1 Fringe Counting

The simplest case of homodyne interferometry is referred to as *fringe counting*. In this technique, the photocurrent *i* drives a counter which triggers on the maxima or minima in the signal (interference fringes) to give a "crude" measure of distance accurate to $\lambda/4$.

A further refinement to this technique involves introducing a phase modulation in one arm of the interferometer. By averaging the fringe count over 1000 cycles for example, a peak-to-peak amplitude of $\lambda/2$ can be measured with a resolution of $\lambda/2000$ (Wolf, 1987).

### 1.6.1.2 Inverse Cosine Method

A second method involves normalizing the photocurrent magnitude with respect to the minimum $(I_{lo} + I_s - 2(I_{lo}I_s)^{1/2})$ and maximum $(I_{lo} + I_s + 2(I_{lo}I_s)^{1/2})$ values of *i* in Equation (1.10). The inverse cosine function is computed to recover the mirror displacement *d*. Kubota *et al.* (1987) report achieving 20 nm accuracies with this technique.

For measurement ranges much less than $\lambda$, a linear relationship between photocurrent amplitude and path length difference is often assumed using the following technique: a $\pi/2$ phase delay is introduced into one of the arms of the interferometer with a retarder plate. The interference term becomes,

$$\cos(2kd + \pi/2) = \sin(2kd) \approx 2kd, \qquad (1.13)$$

for $2kd$ small.

### 1.6.1.3 Closed-Loop Feedback Systems

A third method, referred to as *closed-loop feedback systems* (Hariharan, 1987), is based on phase compensation. Changes in the magnitude of the photocurrent $i$ are detected and fed back to a phase modulator in one of the interferometer arms, so as to hold the amplitude constant. The drive signal of the modulator is then a measure of the path length difference. One advantage of this technique is that the range of measurement can extend beyond one wavelength, depending on the phase modulator.

### 1.6.1.4 Phase Stepping

A fourth type of homodyne technique is referred to as *phase-stepping*. For a given moving mirror position, a series of intensity values are recorded as the path length difference is changed a number of equal steps using a phase modulator. The intensity values can be represented by a Fourier series whose coefficients can be evaluated to obtain the original phase difference between the interfering wavefronts.

A simpler version of this method (Frantz *et al.*, 1979) involves four measurements ($I_1$ to $I_4$) at every $\lambda/4$ phase shifts (including the first measurement at 0° phase). The original phase angle can be recovered by the following,

$$2kd = \tan^{-1} \{ (I_2 - I_4) / (I_1 - I_3) \}. \qquad (1.14)$$

### 1.6.1.5 Quasi-Heterodyne

A fifth method, similar to the previous simplified one is referred to as *quasi-heterodyne*. For a given moving mirror position, the path length difference is varied linearly with time either by introducing a frequency offset between the beams or by means of linear phase modulation. The intensity pattern is integrated over a number of equal segments (typically four) covering one period of the

sinusoidal signal. The original phase can be recovered using Equation (1.14). Stumpf (1979) reports achieving a resolution of 2.5 nm *rms* in a measurement time of 0.6 seconds with this method.

### 1.6.1.6 Laser Feedback Interferometers

A final amplitude encoded information method is known as *laser feedback interferometers*. This extremely simple method makes use of the fact that the intensity of the laser beam can be influenced by feeding a small portion of the output back into the laser cavity. This feedback is provided by an external cavity consisting of the output mirror of the laser and an external moving mirror on the beam axis. The laser output power then varies cyclically with the spacing between the laser output mirror and the moving mirror.

Typically (Wolf, 1987), with a laser mirror having a transmittance of 0.008, the output power can be made to vary by a factor of four by using an external mirror with a reflectance of 0.1. This method, although very simple and very sensitive, has the disadvantage that the response decreases at high frequencies because of the finite time required for the amplitude of the laser oscillation to build up within the cavity. Timmermans *et al.* (1978) report achieving a measurement resolution of 0.1 μm with this method.

## 1.6.2 Phase Encoded Information Techniques

If a fixed frequency shift is introduced into either of the two Michelson interferometer arms (see Figure 1-4), the photocurrent *i* becomes a sinusoid, oscillating at the difference frequency $\Delta\omega = \omega_{lo} - \omega_s$. This is the principle of *heterodyne phase modulated (PM) interferometry*. Here the phase of *i* is directly proportional to optical phase between the interfering wavefonts, and it follows from Equations 1.6 and 1.9 that it is also proportional to *d*. Generally, the difference frequency $\Delta\omega$ ranges from 100 kHz to 100 MHz.

### 1.6.2.1 One Bragg Cell Design

In a first heterodyne PM technique, one of the two interferometer arms is shifted in frequency by $\Delta\omega$ using a device such as an acousto-optic modulator (Bragg cell) driven by a highly stable reference oscillator. The photocurrent *i* and a signal from the reference oscillator are fed to a high precision phase demodulator, where the optical phase is recovered.

This technique, although simple and highly effective, requires the electronic phase demodulation of a radio frequency signal usually in the 40 MHz to 90 MHz range. Royer *et al.* (1985) reportedly achieved measurement resolution results of $10^{-14}$m/Hz$^{1/2}$ with this method, which is very close the theoretical quantum limit.

### 1.6.2.2 Two Bragg Cell Design

In a second heterodyne PM technique (Zhu *et al.*, 1988; Massie, 1987; Smythe *et al.*, 1987), both interferometer beams are shifted in frequency by a different amount, again using devices such as acousto-optic modulators. The photocurrent *i* oscillates at the difference frequency between the Bragg cell reference oscillators, usually in the 100 kHz to 20 MHz range.

A portion of both frequency shifted beams is extracted from the optics prior to the moving mirror section in the interferometer. Both beams are made to interfere on a first detector, where a reference photocurrent $i_r$ is generated at the difference frequency, with a phase which is independent of the moving mirror displacement. The reference $i_r$ and the signal photocurrent *i* from the second detector are then fed to a high accuracy phase demodulator to recover the optical phase.

This technique, although slightly more complex optically than the preceding one, has the advantage that the difference frequency can be decreased to simplify the phase demodulation electronics, at the cost of a reduced bandwidth.

This method is used in the AXIOM 2/20 distance measuring interferometer manufactured by Zygo Corp, for a measurement resolution of 1.25 nm over a range of 5.3 m, at a maximum mirror velocity of 1.8 m/s.

### 1.6.2.3 Zeeman Laser Interferometer

A third technique (Steinmetz *et al.*, 1987; Tanaka *et al.*, 1983), uses the Zeeman effect to generate two laser lines closely spaced in frequency, which are circularly polarized in opposite directions. The frequency separation, which is a function of the applied external magnetic field, can be varied to up to 1.8 MHz in a He-Ne laser. The two beams can be separately launched into the two arms of the interferometer by using a $\lambda/4$ waveplate and a polarizing beamsplitter.

This method also uses two detectors to recover the original phase as in the previous technique. The Hewlett-Packard interferometer, which uses this method, is used widely for industrial measurements accurate to 2.5 nm over a range of 60 m, at a maximum mirror velocity of 0.5 m/s.

The advantage in this case is that the optics are more compact, since no external frequency shifting device is required. However, several authors (Tanaka *et al.*, 1989; Bobroff, 1987; Sutton, 1987), present theoretical and experimental evidence that the imperfect separation of frequencies in the Zeeman laser results in a periodic nonlinearity in the measurements. The nonlinearity has a period of $\lambda$ and can be as large as 12° (20nm) in some cases, depending on the configuration.

### 1.6.2.4 Wavelength Shift Method

Finally, a last heterodyne method makes use of a small induced change in the source laser wavelength from $\lambda$ to $\Delta\lambda$ to measure the path length difference. For a given moving mirror position, the phase of the photocurrent changes by the following amount,

$$\Delta\phi = 4\pi d\,[(1/\lambda) - 1/(\lambda + \Delta\lambda)] \approx 4\pi d\Delta\lambda/\lambda^2 \qquad (1.15)$$

where $\Delta\lambda \ll \lambda$.

Since $\lambda$ and $\Delta\lambda$ are known, the value of *d* can be obtained by measuring the phase shift $\Delta\phi$. The main advantage of this method is its ability to extend the measurement range beyond 1 wavelength of the laser light. Kikuta *et al.* (1986) report achieving <10 um *SD* resolution, over several centimetres of measurement range, with this method.

### 1.6.3 Frequency Encoded Information techniques

In this last category of interferometers, the techniques are actually a hybrid between homodyne and heterodyne designs.

### 1.6.3.1 Fabry-Perot Method

In a first technique, two mirrors are attached to the two points between which measurements are to be made, forming a Fabry-Perot interferometer. The frequency of a first slave laser is locked to a transmission peak of the interferometer, so that the wavelength of the slave laser is an integral submultiple of the path length difference.

Any change in the separation of the mirrors then results in a corresponding change in the wavelength of the slave laser and hence in its frequency. These changes can be measured by mixing the beam from the slave laser at a photo-detector with the beam from a second reference laser, and measuring the beat frequency. Jacobs *et al.* (1984) use this method for measuring thermal expansion of 100 mm samples to a resolution of 1 nm.

### 1.6.3.2 FMCW

In another technique, known as *Frequency Modulation Continuous Wave (FMCW)* or *frequency shift keying*, the source laser is frequency modulated in a repeating ramp fashion (Economou *et al.*, 1986; Beheim *et al.*, 1985). The photocurrent *i* at the detector is a beat signal at the difference frequency resulting from the mixing of the frequency ramp with a delayed version of itself. The frequency of the beat signal is proportional to the delay in the path length of the light between the two interferometer arms. Economou *et al.* (1986) report a measurement resolution of 2 μm over a range of 60 mm, in a bandwidth of 100 kHz, using this method.

## 1.7 Choice of Interferometry Technique

In theory, both homodyne and heterodyne interferometers can attain similar levels of accuracy of around $10^{-15}$m•Hz$^{-0.5}$ (Wagner *et al.*, 1987). This is more than sufficient for our design objective of $10^{-12}$m•Hz$^{-0.5}$.

However, practical considerations such as noise, optics efficiency, alignment, electronics and sensitivity to the environment combine to degrade the actual performance of the interferometer. The results are often far from the theoretical quantum limit, as confirmed by the experimental results in the literature. Table 1-3 summarises and compares the more important parameters in the reported performance of the techniques outlined above.

Note that many of the interferometry methods described above for subwavelength resolution (known as *interpolation* methods) have a measurement range which is less than one wavelength. However, most of these methods can usually be combined with some form of fringe counting to extend the range of measurement to several wavelengths. For this reason, the measurement range is not included as a parameter in Table 1-3.

The first design criteria for our interferometer is that the bandwidth be "high" (6 MHz) and that the resolution also be "high" (1 nm), as defined in Table 1-3. This eliminates all but the homodyne *inverse cosine* method and the first three heterodyne methods.

As noise and adverse environmental conditions affect the different techniques described above to varying degrees, the choice of a particular technique must also be based on practical considerations and the expected operating environment of the interferometer.

Hence, the second design criteria for the interferometer is that the optics be simple and compact to minimize the effects of adverse environmental conditions and to keep costs down. As the micro-robot requires 3 interferometers per limb, the cost per transducer must be kept low.

| METHOD | BW | RES. | COMMENTS |
|---|---|---|---|
| **- Amplitude Encoded Information -** | | | |
| Fringe averaging | low | high | Simplest |
| Inverse cosine | high | high | Complex to elim. laser power noise |
| Closed loop fbk | med | high | Range > λ |
| Phase Stepping | med | ? | |
| Quasi het. | low | high | |
| Laser feedback | med | low | Very Simple |
| **- Phase Encoded Information -** | | | |
| 1 Bragg cell | high | high | Simple, but high frequency phase signal |
| 2 Bragg cells | high | high | More complex, but lower frequency signal |
| Zeeman laser | high | high | Compact, but periodic non-linearity |
| Wavelength shift | high | low | |
| **- Frequency Encoded Information -** | | | |
| Fabry-Perot | ? | high | Two lasers, BW low for range > λ |
| FMCW | med. | low | Absolute distance measure |

**LEGEND**

BW (Bandwidth)
- low: DC to 1 kHz
- med: 1 kHz to a 2 MHz
- high: > 2 MHz

Res (Resolution)
- low: > 1 μm
- med: 1 μm to 5 nm
- high: < 5 nm

**Table 1-3.** Comparative listing of the various interferometry techniques encountered in the literature.

Homodyne interferometers are often desirable because of the simplicity of the optics and the electronic design, and the associated low cost. The most serious drawback with homodyne techniques however is that they are very sensitive to the common problem of laser output power fluctuations.

As the information is amplitude encoded, any spurious fluctuation in the source laser power will be interpreted as a signal. In Equation (1.10) for example, any undesirable variation in $I_{lo}$ or $I_s$ will be indistinguishable from actual changes in $d$ reflected in the information carrying $cos(2kd)$ term.

In order to overcome this problem, elaborate optics schemes have been proposed to improve the basic inverse cosine homodyne interferometer design, such as Yang *et al.* (1987), who report a resolution of $10^{-12}m \cdot Hz^{-0.5}$, in a measurement range of less than one wavelength.

In heterodyne interferometry however, the effect of small variations in laser output power on the recovered optical phase signal can be practically eliminated by simple methods in the electronics. There is no need for complex optical solutions to the problem.

Heterodyne interferometers are also better suited for electrically and optically noisy environments, as they provide higher discrimination against background noise (Delange, 1968). Hence for high accuracy interferometers, heterodyne systems are a better choice.

Finally, because of the available consulting expertise in high frequency electronics at MPB Technologies Inc. and the desirable simplicity of the one Bragg cell heterodyne design, this technique was chosen for our system. The Zeeman laser technique was eliminated due to the non-linearity problems and the high cost of the laser ($10,000). The details of our design are described in the next chapter.

# CHAPTER TWO: INTERFEROMETER DESIGN

In this Chapter the design of three different sections of the interferometer is described: optics, electronic phase demodulator and computer phase to displacement conversion algorithm.

The interferometer was designed to meet the specifications for the two limb displacement velocity modes ("high speed/low accuracy" and "low speed/high accuracy"), for experiment durations of 1 second, in the following way: First, the device measures path length differences with a resolution < 1 nm SD at frequencies from DC to 100 kHz, using fringe interpolation; Secondly, the device measures displacements by fringe counting when the micro-robot limbs are moving at higher velocities. The maximum limb displacement speed (2 m/s) corresponds to a He-Ne fringe rate of 6.3 million fringes per second, or a bandwidth of 6.3 MHz.

In the last section of the chapter, a derivation of the theoretical minimal detectable displacement for the interferometer is presented.

## 2.1 Optics Design

As explained in the previous chapter, the laser interferometry technique that best fits the design criteria is the "one Bragg cell" heterodyne method. The design, partially based on a method proposed by Royer *et al.* (1986), is shown in Figure 2-1. A photograph of the setup is shown in Figure 2-2.

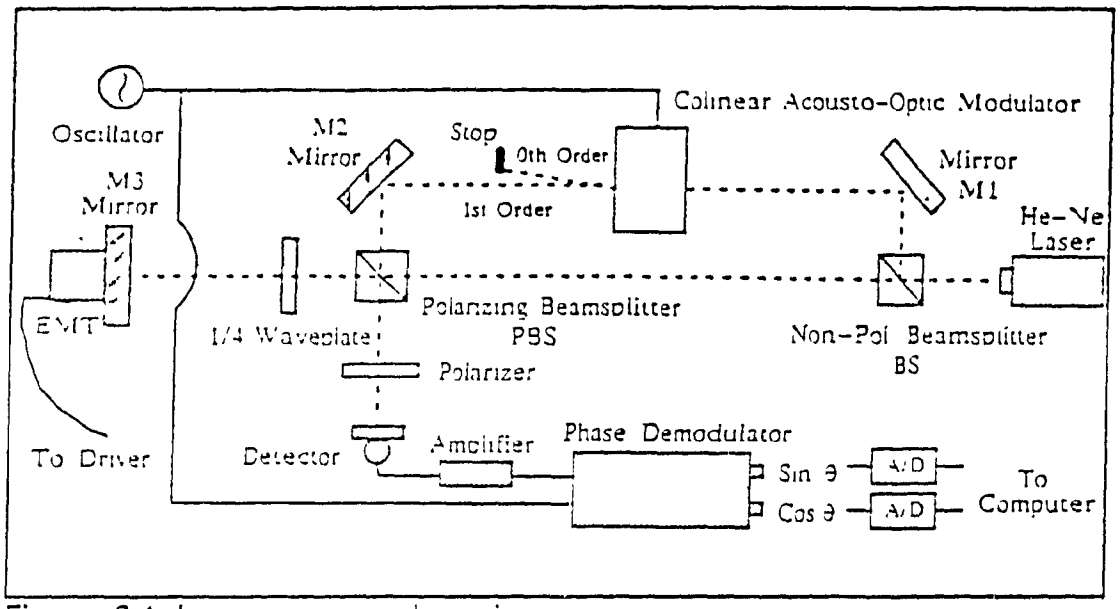


Figure 2-1. Interferometer schematic.

The source laser beam, linearly polarized in the plane parallel to the surface of the optical table, is first split by the 50/50 non-polarizing beam splitter. The *local oscillator* beam of the interferometer is reflected off mirror M1 and goes through the collinear acousto-optic modulator, where it is shifted in frequency. The beam is then reflected off mirror M2, goes through the polarizing beam splitter and the linear polarizer, and finally onto the detector.

The *signal* beam of the interferometer first goes through both beam splitters, through the 1/4 waveplate, and is then reflected off the moving mirror M3. This mirror is mounted on an electromechanical translator (EMT) which is used to displace the mirror along the axis of the beam. When the signal beam returns to the polarizing beam splitter, the two passes through the 1/4 waveplate have shifted the polarization angle by 90°.The beam is thus deflected by the polarizing beamsplitter, and passes through the linear polarizer to the detector.

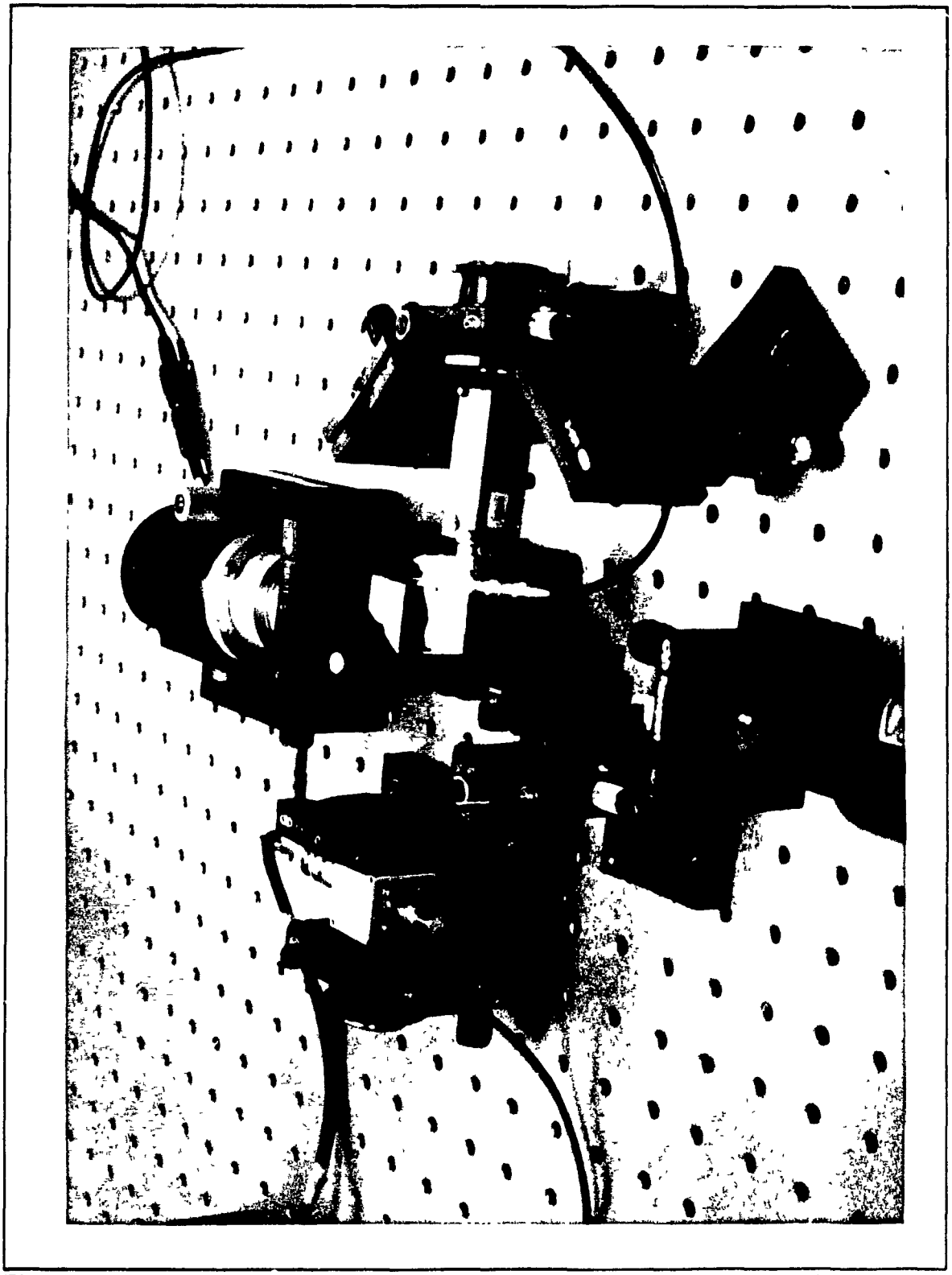

**Figure 2-2.** Photograph of the interferometer layout on the optical table

The polarizer axis is oriented at 45° with respect to the plane of the optical table. This allows the local oscillator and signal beams, which are mutually orthogonally polarized, to interfere on the detector. The photocurrent from the detector is then pre-amplified and sent to the phase demodulator

A phase demodulator, designed and built for this project (see Section 2.2), takes as input the pre-amplified photocurrent from the detector and the Bragg cell reference oscillator. The circuit outputs two signals which are proportional to the sine and cosine of the phase angle between the inputs. The dual outputs are then analog to digital converted for processing by a computer. The details of the electronics and computer processing are explained in later sections.

The setup is mounted on an optical table (Newport model RS-510-12), which isolates the interferometer from ground and building mechanical vibrations. The setup in also enclosed in a padded chamber, for isolation from sound vibrations and thermal perturbations.

The main reason for selecting this design over other available "one Bragg cell" heterodyne designs is its effective isolation of the laser from back-reflections. In precision interferometers, special care must be taken to avoid optical feedback of light from the interferometer back into the laser cavity (back-reflections). Changes in the amplitude or the phase of the reflected light can cause changes in the output power and the frequency of the laser (Hariharan, 1987; Wolf, 1987; Royer *et al.*, 1985).

This design incorporates several features to minimize reflections of light from the interferometer back into the laser cavity. First, back-reflections from the local oscillator beam are limited by the Bragg cell, and back-reflections from the signal beam are limited by the combination of the 1/4 waveplate and the polarizing beamsplitter.

Secondly, the optics have an anti-reflection coating for the He-Ne laser wavelength. Lastly, the optics are purposely skewed such that the laser beam is never normally incident onto any component surface (not shown in Figure 2.1).

In this way, any residual back-reflections are directed outside of the interferometer.

### 2.1.1 Probe Laser Selection

A 5mW linearly polarized He-Ne laser (Melles-Griot model 05-LHP-151) was selected as a source for the interferometer. The principal line of the He-Ne laser is in the visible range (632.8 nm), and such lasers are readily available at low cost. The coherence length is typically 0.2 to 0.3 m, which is sufficient to accommodate the required 0.01 m range of the design.

### 2.1.2 Frequency Shifter Selection

A 70 MHz acousto-optic cell (Isomet Corp model 1205C-1-794) was selected to shift the frequency of the local oscillator arm in the interferometer, because of the high quality and ready availability of Bragg cells. Under optimal alignment conditions, 80% of the incident light is diffracted into the first order output (frequency shifted) beam.

Also, the frequency of the acousto-optic (Bragg) cell is the upper bound on the measurement bandwidth of the interferometer. Hence, the 6.3 MHz bandwidth corresponding to the maximum limb displacement speed is the minimum requirement for the frequency shift. Therefore a 70 MHz frequency shift is more than adequate for this design.

### 2.1.3 Detector and Pre-Amplifier Selection

The detector and pre-amplifier are crucial to the overall interferometer sensitivity and they must be selected with care. A Si avalanche photodiode (RCA model C30817) was selected as a detector because of its high quantum efficiency at 632.8 nm (60% - 70%), and its adjustable internal current gain (up to 30 dB).

Because of these features, the Si APD is well suited to the detection of weak signals, limited only by the optical quantum noise due to the light incident onto the detector. The pre-amplifier selected was a 35 dB (decibel) gain, 2 dB noise figure low noise amplifier (Miteq model AU-3A-000110).

## 2.2 Electronics

The phase demodulator electronics, shown schematically in Figure 2-3, were designed to take two 70 MHz inputs and provide outputs proportional to the sine and cosine of the instantaneous phase between the inputs, for a phase modulation bandwidth of 1 DC to 6 MHz. The electronics were assembled on a prototype board with a ground plane on one side.

The circuit was tested independently from the optics for calibration, frequency response, and sensitivity to input noise, as explained in the following sections. Many of the design techniques were taken from Horowitz and Hill (1989) for the low frequency electronics, and from Bowick (1986) for the radio frequency electronics.

### 2.2.1 Electronics Design

The RF (radio frequency) signal from the detector (SIG) is routed to a 0° power divider (Mini-Circuits model MSC-2-1W) and then to highspeed comparators (Plessy model SP9680). The comparators convert the input RF sinusoids to square waves, where the square wave amplitude is constant and independent of the input amplitude. The comparators protect the phase detectors (Mini-Circuits model MPD-1) from any fluctuations in the input amplitude. The interferometer as a whole is thus isolated electronically from any power fluctuations of less than 20% in the source laser.

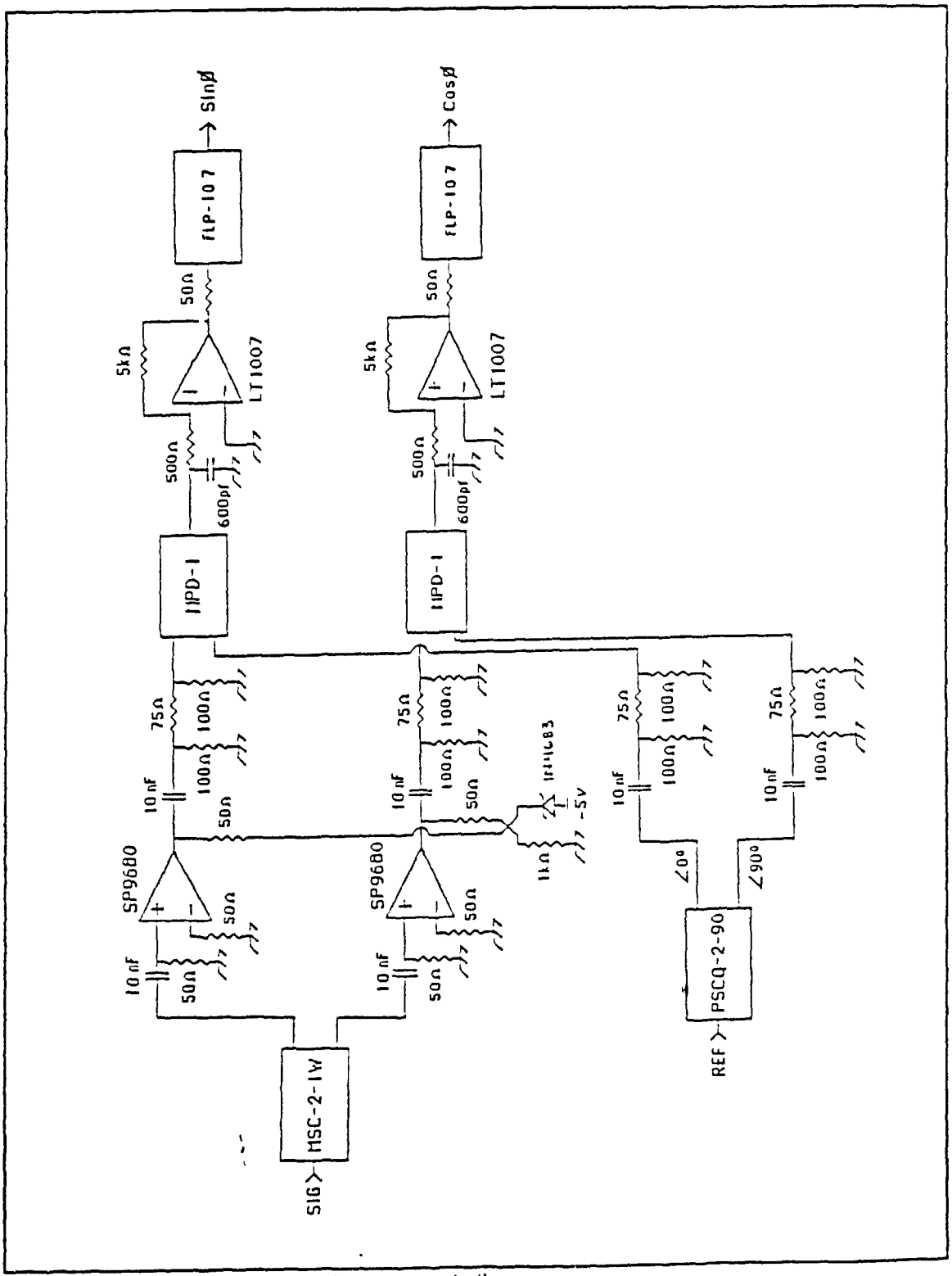


Figure 2-3. Phase demodulator circuit diagram.

The RF reference signal from the Bragg cell oscillator (REF) is routed to a 90° power divider (Mini-Circuits model PSCQ-2-90). The outputs from the comparators and the 90° power divider are fed through 10 dB attenuators to two high frequency phase detectors. The attenuators considerably weaken any reflections between the high frequency components due to impedance mismatch.

The output from the phase detectors are buffered and amplified using low noise operational amplifiers, then low-pass filtered using 10 MHz cutoff third-order Butterworth filters (Mini-Circuits model FLP-10.7)

The outputs from the phase demodulator circuit are in quadrature (90° out of phase with respect to each other). Since sine and cosine are multivalued functions, the direction of displacement cannot be determined uniquely from either function. The combination of both is necessary to determine displacement and direction of motion. In many other interferometer designs, the quadrature is done optically, thus requiring a second photo-detector and assorted electronics.

The RF signal input (SIG) can accept a maximum signal power level of 15 dBm (decibels, referenced to milliwatts). The minimum input power level depends on the desired output signal to noise ratio (SNR), see Section 2.4. The RF reference input (REF) can accept a maximum signal power of 30 dBm. Up to about 20 dBm input power, the output signal power of the demodulator is directly proportional to the input RF reference signal power. Beyond this point however, the output signal level stabilizes at roughly 4 Vpp (peak-to-peak), as the diode bridge in the phase detectors is saturated.

### 2.2.2 Frequency Response

The electronics were required to have a flat frequency response at least up to 100 kHz for high accuracy fringe interpolation in the "low speed / high resolution" mode of the interferometer. Between 100 kHz and 6 MHz, in the "high speed / low resolution" mode, the frequency response characteristics are less critical, as fringe counting only is used for a "crude" measure of displacement.

The frequency response of the phase demodulator electronics was determined using the configuration shown in Figure 2-4. The output of a 70 MHz reference oscillator is split by a 0° degree power divider and both output signals are routed to the phase demodulator. The phase of one of the inputs is modulated by a voltage controlled phase shifter (Merrimac model PSE-4-70). A dynamic signal analyzer (Hewlett-Packard model HP3262A) is used to compute the frequency response between the modulation input to the phase shifter and the outputs from the phase demodulator, over the frequency range of interest.

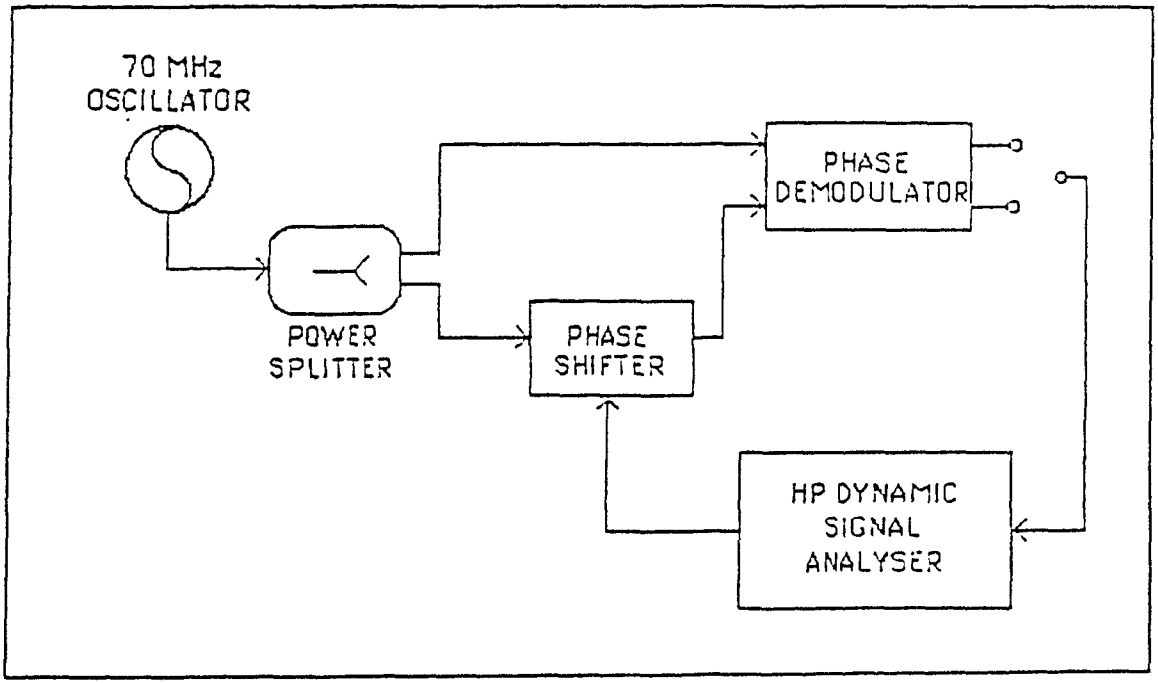


Figure 2-4. Frequency response test measurement setup.

Unfortunately, the best available electronic phase shifter that could be found was limited to a modulation bandwidth of about 10 kHz. Hence it is expected that the results of the frequency response computation will be limited by this component in the measurement setup.

The magnitude and phase portions of the computed Bode plot are shown in Figures 2-5 and 2-6. The response is a low-pass with a roll off around 10 kHz, as expected. The coherence function (Bendat & Piersol, 1980), shown in Figure 2-7, demonstrates that the system exhibits a high degree of linearity across the frequency range of measurement.

This exercise demonstrates that the response of the phase demodulator electronics is flat to at least 10 kHz, hence over most of the required "low speed / high resolution" mode range. It is expected that the actual response of the demodulator is flat to about 2 MHz (bandwidth of the output stage op-amps). This will be extended in a future version of the design, as explained in Chapter four.

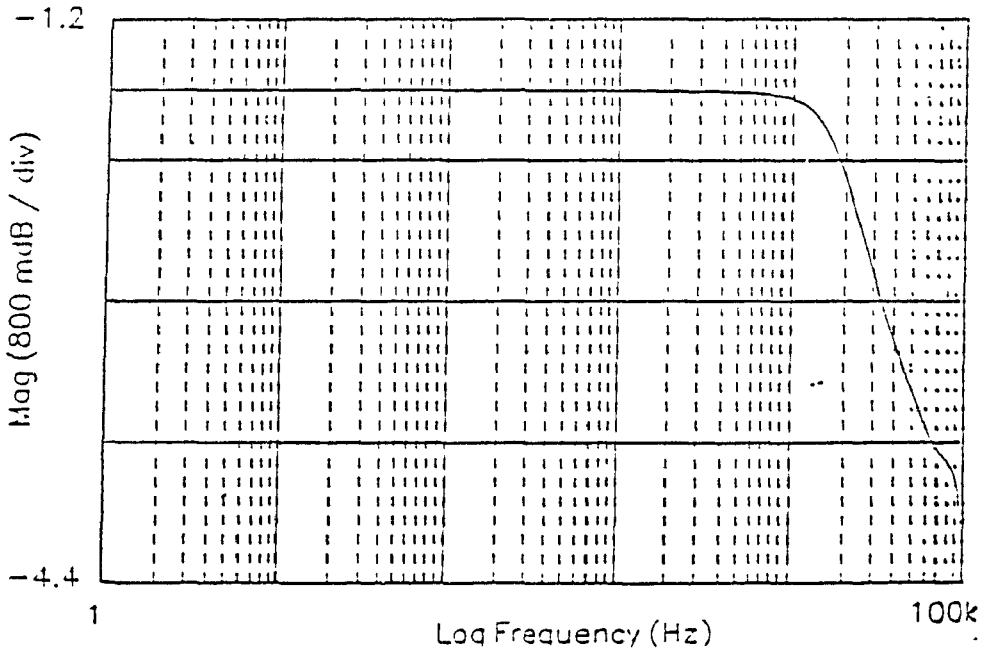


**Figure 2-5.** Plot of the frequency response of the phase demodulator electronics: magnitude portion of the Bode plot.

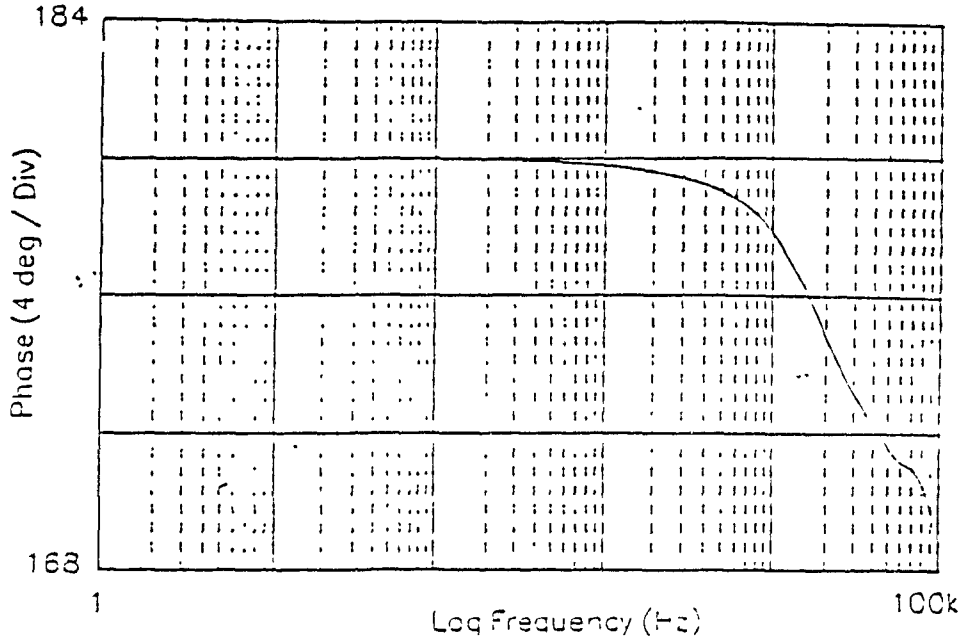


**Figure 2-6.** Plot of the frequency response of the phase demodulator electronics: phase portion of the Bode plot.

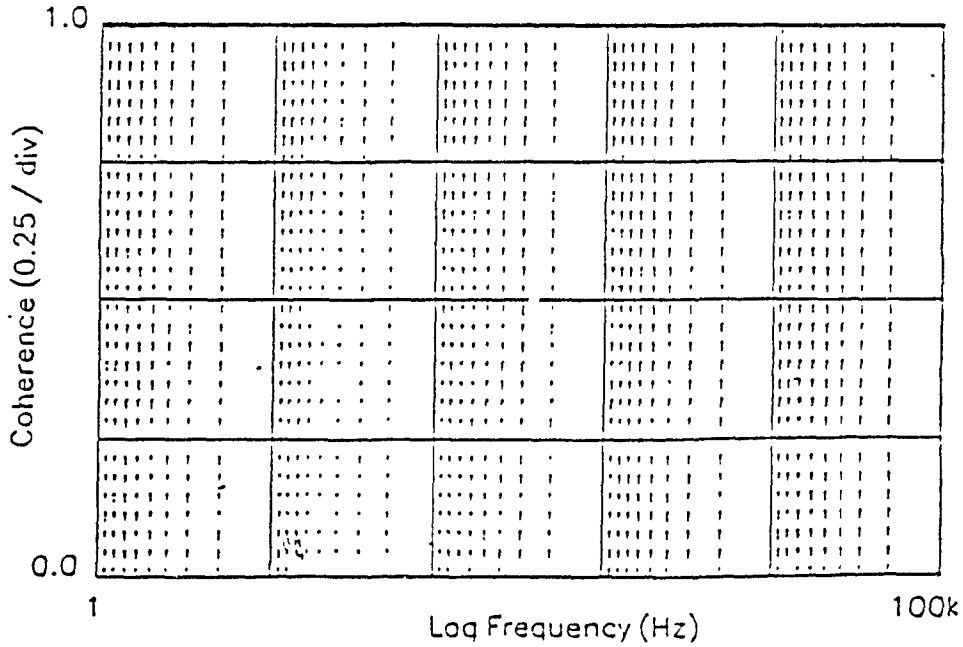


**Figure 2-7.** Plot of the frequency response of the phase demodulator electronics: coherence function.

### 2.2.3 Thermal Sensitivity of the Electronics

In order to determine qualitatively the sensitivity of the electronics to thermal perturbations, the following experiment was conducted: both phase demodulator inputs were connected to the Bragg cell oscillator, forcing the circuit to output a constant voltage on both output ports. Directing the "spray" of a heat gun onto the circuit caused the output signal levels to vary instantly over several "virtual" fringes.

In order to reduce the sensitivity of the electronics to sudden temperature variations, the circuit was inclosed in a sealed aluminium box, and the experiment was repeated. In this case, the box had to be heated for several minutes before the output signal levels changed perceptibly, thus demonstrating that the box is an effective protection against sudden thermal shock.

For complete isolation from low frequency room temperature variations, the electronics would have to be temperature controlled. However, as experiments with the micro-robot are usually only a few seconds in length, this will not be necessary.

### 2.2.4 Calibration

Because of inevitable imperfections and imbalances in the electronic components, the outputs of the phase demodulator are not perfect sine and cosine functions. For high accuracy phase measurements (ie: $< 5°$), the output functions must be determined exactly.

To determine the output functions, an experiment was conducted where the Bragg cell oscillator was again connected to both inputs of the phase demodulator, as in Figure 2-4, without the dynamic signal analyzer. While using a network analyzer (Hewlett-Packard model HP 8753C) to measure the instantaneous phase between the inputs of the demodulator, the phase offset was smoothly varied from 0° to 360° with the phase shifter.

The value of both phase demodulator outputs were recorded at every 1° phase increment between the inputs. The resulting data is plotted out as a calibration curve in Figure 2-8. The curve will be used by the computer to determine the instantaneous phase angle between the inputs, as explained in the next section. Note that the measurement accuracy of the HP8753C network analyzer is better than 1°.

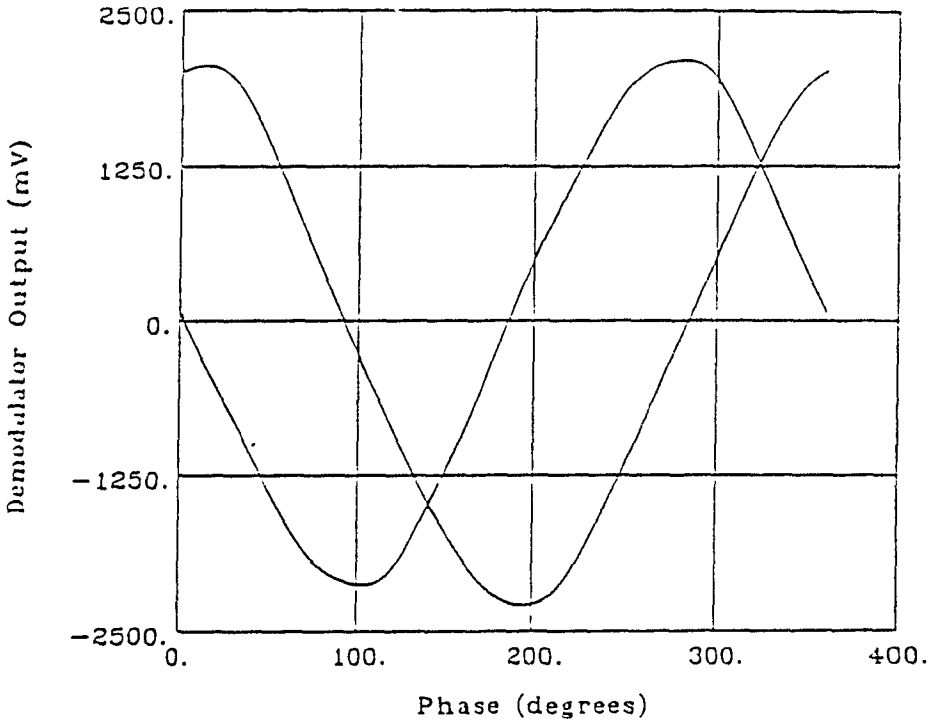


**Figure 2-8.** Plot of the voltage versus phase calibration data for both demodulator outputs, obtained by varying the phase between the inputs from 0° to 360° in increments of 1°.

## 2.3 Computation of Displacement by Computer

As explained above, in order to achieve phase measurement accuracies of 5° or better, the phase must be determined using the calibration data. This is best accomplished by a computer with a lookup table. Note that the computer programs written in QuickBasic (Microsoft Corp., 1989) to execute the tasks described in this section are included in the Appendix.

Firstly, note from either curve in Figure 2-8 that every voltage value on the $y$ axis corresponds to two possible phase angles on the $x$ axis (ie: sine and cosine are dual valued functions).

Secondly, note that the uncertainty on the data in the calibration curve is inversely proportional to the magnitude of the instantaneous slope. To understand this, let small changes in phase $\Delta\phi$ and in voltage $\Delta v$ be related by,

$$\Delta v = m\Delta\phi, \tag{2.1}$$

where $m$ is the instantaneous slope.

For a fixed measurement uncertainty in voltage $\Delta v$, the corresponding uncertainty in phase is lowest when $m$ is largest, and the uncertainty is huge when $m \sim 0$. In other words, the uncertainty is greatest at the extrema, and lowest around the zero crossings. Since both curves are arranged in quadrature, the uncertainty on one curve is greatest when the uncertainty on the other is lowest.

This property is used to minimize the uncertainty in the phase to displacement conversion process with the calibration data. The sine and cosine curves are used separately to recover the phase angle from the calibration data. A weighted sum of both results is used to compute the final angle estimate, where the weights are functions of the slopes. Note that the uncertainty on the weighted sum is greatest around multiples of 45° because the uncertainty on both angle estimates are roughly equal.

The lookup table structure is shown in Figure 2-9. The table contains 5,000 rows of 5 columns each. There is a row for every output voltage value between 2.5 V and -2.5 V, in increments of 1 mV. Each row contains the pairs of possible angles for both output channels, at that particular output voltage: in columns 1 & 2 for channel 1 (sine), and in columns 3 & 4 for channel 2 (cosine). Finally, in column 5 of each row is stored a value which approximates the slope at that particular voltage on both curves.

The algorithm for computing the phase angle between the inputs for any pair of output voltage values (*v1* and *v2*) is as follows:

*if (v1 "same sign as" v2)*
*then*

$$angle = [ (A_{11} * W_1) + (A_{21} * W_2) ] / [W_1 + W_2]$$

*else*

$$angle = [ (A_{12} * W_1) + (A_{22} * W_2) ] / [W_1 + W_2]$$

*endif*

*where:*

$A_{11} = Table(v_1, 1)$
$A_{12} = Table(v_1, 2)$
$W_1 = Table(v_1, 5)$

$A_{21} = Table(v_2, 3)$
$A_{22} = Table(v_2, 4)$
$W_2 = Table(v_2, 5)$

Note that the angle estimate pairs $A_{11}$ & $A_{21}$ or $A_{12}$ & $A_{22}$ are multiplied by the weights $W_1$ and $W_2$. The weights are inversely proportional to the uncertainty on the voltage measurements $v_1$ and $v_2$, as explained earlier. For example if $v_1 \approx 0$ V, then $W_1 \approx 1$ and $W_2 \approx 0$. Thus the $v_2$ output is virtually ignored from the angle computation because the uncertainty on this measurement is comparatively large.

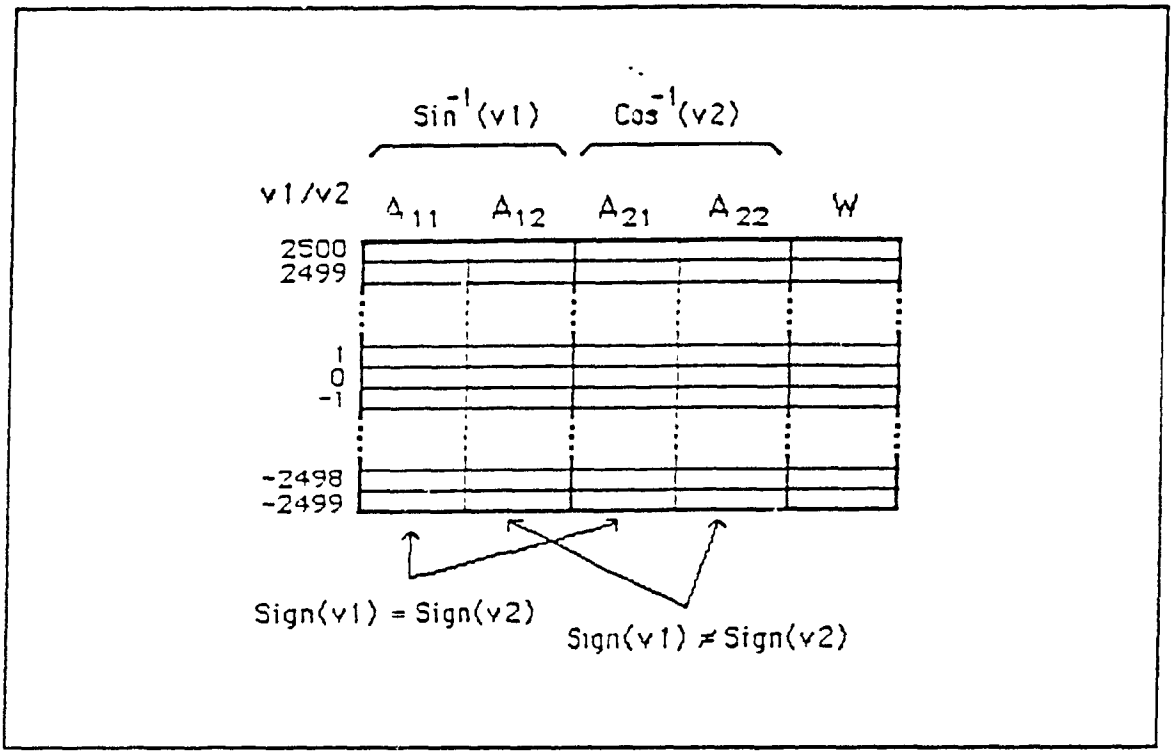


Figure 2-9. Structure of the lookup table used by the computer for the phase to displacement conversion.

Conversely, if $v_2 \approx 0$ V, then $W_1 \approx 0$ and $W_2 \approx 1$. In this case the $v_1$ measurement is virtually ignored from the angle computation. Also, if the phase angle between the inputs is a multiple of 45°, the uncertainties on the voltage measurements are equal ( $|\mathrm{Sin}(n*45°)| = |\mathrm{Cos}(n*45°)|$ ), thus $W_1 = W_2$.

The actual displacement corresponding to a particular phase angle is computed using Equations 1.6 and 1.9. Whenever the computed phase angle crosses 0° or 360°, a simple algorithm adds or subtracts $\lambda/2$ from the current position, according to the direction of motion. This is in fact a method of fringe counting which extends the measurement range over many wavelengths (theoretically to the coherence length).

Note finally that the calibration data does not contain enough points to fill the lookup table entirely. In fact there are only 360 * 2 calibration data points, and 5,000 * 5 lookup table entries. The lookup table is actually filled in two passes. In the first pass, the calibration data is entered in the appropriate rows in the table. In the second pass, the empty rows are filled with a copy of the nearest calibration data row from the first pass.

Hence to summarize: prior to an experiment, a lookup table is built in two passes in the computer memory. For a series of measurements, both outputs from the phase demodulator are fed to A/D converters. The computer reads the contents of the A/Ds and computes the actual mirror movement by estimating the phase angle using the lookup table and computing the corresponding displacement using Equations 1.6 and 1.9.

## 2.4 Minimal Detectable Displacement

In this section, the expression for the minimal detectable displacement by the interferometer is derived, and the expected result for the experimental conditions of Chapter three is computed.

The underlying principle for the computation is the estimation of the carrier to noise ratio (*CNR*) for the input signal to the phase demodulator, and the resulting signal to noise ratio (*SNR*) at the output of the demodulator.

The *rms* output noise power $N_o$ within a bandwidth $B$ from the detector/pre-amplifier combination, modelled by (Webb *et al.*, 1974) is,

$$N_o = G\{N_D + \langle i_A^2 \rangle R_L\}, \tag{2.2}$$

where $N_D$ is the photo-detector *rms* noise power output within a bandwidth $B$, $G$ is the pre-amplifier gain, and $\langle i_A^2 \rangle$ is the equivalent mean-square noise current of the pre-amplifier and its load resistor $R_L$.

The *rms* noise power from the pre-amplifier and its load resistor is thermal in origin and is calculated with,

$$\langle i_A^2 \rangle = \{ 4k(T_o + T_e)B \} / R_L, \quad (2.3)$$

where $k$ is Bolzmann's constant ($1.37 \times 10^{-23}$ J/K), $T_e$ is the equivalent amplifier temperature, and $T_o$ is the load resistor temperature (usually the room temperature, 293 K). The equivalent amplifier temperature $T_e$ is normally specified in terms of the amplifier noise figure $F$ defined as,

$$F = 10\log\{1 + (T_e / 293\ K)\}\ (dB). \quad (2.4)$$

The *rms* output noise power $N_D$ for a P-I-N or avalanche-type photodiode is calculated using (Webb *et al.*, 1974),

$$N_D = 2e\{I_{ds} + (\langle P_o \rangle R_o F_s + I_{db} F_d) M^2\} B R_L, \quad (2.5)$$

where,

- $I_{ds}$ = unmultiplied component of the dark current (usually the surface component),
- $\langle P_o \rangle$ = average optical power incident onto the detector.
- $R_o$ = unity gain responsivity of the detector (A/W),
- $F_s$ = detector effective excess noise factor appropriate to the multiplication of the photocurrent,
- $I_{db}$ = multiplied component of the dark current (usually the bulk component),
- $F_d$ = detector effective excess noise factor appropriate to the multiplication of the dark current $I_{db}$,
- $M$ = internal gain of the detector ($M$ = 1 for a P-I-N).

Note that the term $\langle P_o \rangle R_o F_s$ in Equation 2.5 originates from the uncertainty in the photon to electron conversion process in the detector. This noise term is referred to as *optical shot noise*, and will be discussed in detail below.

For a typical reach-through silicon APD (Webb *et al.*, 1974), the following approximation can be made,

$$F_s \sim F_d \sim k_e M + (2 - 1/M)(1 - k_e), \tag{2.6}$$

where $k_e$ is the effective weighted ionization ratio and depends on the type of diode. For the our APD (RCA model C30817), $k_e = 0.02$.

Equations 2.2 to 2.6 can be combined to express the total *rms* noise power output from the detector/pre-amplifier combination, as shown below,

$$N_o = G\{2eI_{ds} + 2e(\langle P_o \rangle R_o + I_{db})F_d M^2 + [4k(T_o + T_e)/R_L]\}BR_L. \tag{2.7}$$

The highest possible accuracy is achieved in an interferometer when the optical shot noise is the dominating noise source in the system. Hence, for optimum performance, the average optical power $\langle P_o \rangle$ and the internal gain $M$ must be adjusted such that the shot noise term $G2e\langle P_o \rangle R_o F_d M^2 BR_L$ dominates over the other noise terms in Equation 2.7.

The first and third noise terms within the curly brackets in Equation 2.7 are constant for a particular combination of detector, amplifier and load resistor. The second term however is proportional to the square of adjustable internal gain. By increasing $M$ sufficiently, the second term in Equation 2.7 will dominate Note that this adjustment is not possible with a detector with no internal gain, such as a P-I-N Si photodiode.

Furthermore, within the second term, the average incident optical power $\langle P_o \rangle$ can be increased until the shot noise dominates over the multiplied dark current $I_{db}$. Under such conditions, the total *rms* noise power expression reduces to Equation 2.8 and the system is said to be *shot noise limited*,

$$N_o = 2e\langle P_o \rangle R_o F_d M^2 BR_L G. \tag{2.8}$$

This procedure is accomplished experimentally by looking at the frequency content of the photocurrent on a spectrum analyzer. For a given incident optical power $\langle P_o \rangle$ onto the detector, the APD gain $M$ is increased until the noise floor on the spectrum analyzer starts to increase. At this point, the optical shot noise dominates over other noise sources. The procedure is confirmed by blocking the light beam in front of the detector and verifying that the noise floor drops to some lower value.

The parameters for the experiments described in Chapter three are listed below. The magnitude of the various noise components in Equation 2.7 are compared and the photocurrent signal is verified to be shot noise limited.

Experimental conditions:

| | | | |
|---|---|---|---|
| $e$ | $= 1.6 \times 10^{-19}$ c, | $I_{db}$ | $= 9.4 \times 10^{-8}$ A, |
| $I_{ds}$ | $= 7.9 \times 10^{-11}$ A, | $T_e$ | = 293 K, |
| $T_o$ | = 293 K. | $R_L$ | = 20 Ω, |
| $\langle P_o \rangle$ | = 0.602 μW *rms*, | $R_o$ | = 0.35 A/W, |
| $F_d$ | = 3.47 (for $M$ = 76), | $M$ | = 76, |
| $B$ | = 10 kHz, | $G$ | = 35 dB. |

From equation 2.7:

| | |
|---|---|
| 1) $2e\langle P_o \rangle R_o F_d M^2 G B R_L$ | $= 2.137 \times 10^{-12}$ W *rms* |
| 2) $2eI_{ds} G B R_L$ | $= 39.97 \times 10^{-21}$ W *rms* |
| 3) $2eI_{db} F_d M^2 G B R_L$ | $= 953.1 \times 10^{-15}$ W *rms* |
| 4) $4k(T_o + T_e) G B$ | $= 1.015 \times 10^{-12}$ W *rms* |

Hence the photocurrent signal from the detector will be shot noise limited since the shot noise component (#1 above) is greater than the sum of the other noise components.

The photocurrent *rms* signal power $P_i$ from the detector is computed using,

$$P_i = \langle i_s \rangle^2 R_L = P_{lo} P_s R_o^2 M^2 G R_L, \quad (2.9)$$

where,

$\langle i_s \rangle$ = Time averaged photocurrent from the detector,
$P_{lo}$ = Local oscillator beam *rms* optical power incident onto the detector,
$P_s$ = Signal beam *rms* optical power incident onto the detector.

Experimental conditions,

$P_{lo}$ = 0.346 μW *rms*,
$P_s$ = 0.256 μW *rms*.

From Equation 2.9,

$P_i$ = $9.9 \times 10^{-6}$ W *rms*.

Combining Equations 2.7 and 2.9, the power carrier to noise ratio $CNR_p$ for the shot noise limited photocurrent from the detector/pre-amplifier combination can be computed as,

$$CNR_p = P_i / N_o$$
$$= \{P_{lo} P_s R_o^2 M^2\} / \{2el_{ds} + 2e(\langle P_o \rangle R_o + I_{db}) F_d M^2 + [4k(T_o + T_e)/R_L]\} B \quad (2.10)$$
$$= 64 \text{ dB, for the experimental condition of Chapter three.}$$

To summarize the equations for the detector/pre-amplifier section, the $CNR_p$ is maximized for a given bandwidth $B$ by increasing the internal gain $M$ and the incident optical power $P_o$, until the system is shot noise limited. Note that any increase in $M$ beyond this point however will only decrease the $CNR_p$ through an increase in $F_d$ .

The next step in the derivation is to consider the effect of the phase demodulator. Assuming the input photo-current $i_s(t)$ to the phase demodulator is a signal of the form,

$$i_s(t) = A_c cos[\Delta\omega t + m_s sin(\omega_s t)] + n(t), \quad (2.11)$$

where,

$A_c$ is the carrier amplitude,
$\Delta\omega$ is the carrier frequency,
$m_s$ is the modulation amplitude,
$\omega_s$ is the modulation frequency,
$n(t)$ is additive Gaussian noise (the shot noise in this case),

then the demodulator output *rms* power $P_o$ and output noise *rms* power $N_i$, due to $n(t)$, can be expressed as (Haykin, 1983),

$$N_i = k_p^2 / R_L CNR_p, \quad (2.12)$$

and,

$$P_o = (km_s)^2 / 2R_{Lo}, \quad (2.13)$$

where,

$k_p$ is the phase sensitivity of the demodulator (V/rad),
$R_{Lo}$ is the load resistor at the output.

Furthermore, the demodulator generates an intrinsic noise component $N_d$ which is thermal in origin. Hence the demodulator output power $SNR_p$ between the total output noise and the output signal $P_o$ is,

$$SNR_p = [(k_p m_s)^2/2R_{Lo}] / \{[k_p^2/R_{Lo}CNR_p] + N_d\} \quad (2.14)$$

The intrinsic demodulator noise power $N_d$ is difficult to predict theoretically, so it must be determined experimentally.

For this purpose, an experiment was conducted where a phase modulated signal with a known $CNR_p$ was fed to the RF signal input of the phase demodulator. The RF reference input was connected to the Bragg cell oscillator. The input $CNR_p$ was varied in equal increments over a given range, while the output $SNR_p$ was measured on a spectrum analyzer (Hewlett-Packard model 8568B) at the output ports of the phase demodulator. The results for a resolution bandwidth of 10 kHz on the spectrum analyzer are shown in Figure 2-10.

In the experiment, the input $CNR_p$ was increased from 35 dB to 85 dB. For an input $CNR_p$ below 75 dB, the input signal noise $N_i$ dominated the denominator in Equation 2.14 and the output $SNR_p$ varied linearly with the input. Above 75 dB however, the demodulator noise $N_d$ starts to dominate and the curve flattens, as the output $SNR_p$ no longer followed the input $CNR_p$.

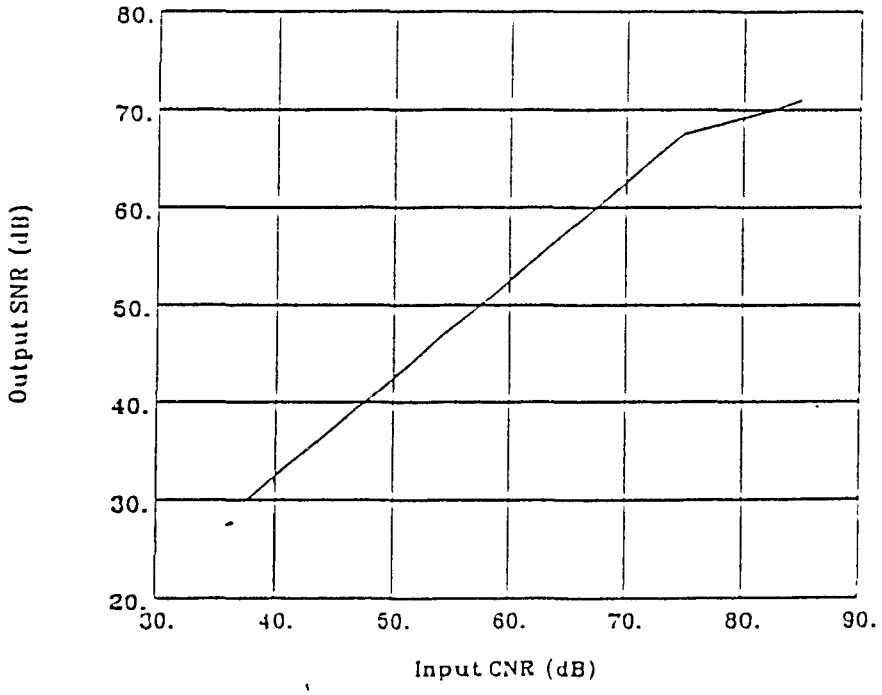


**Figure 2-10.** Experimental data plot of the output SNR versus the input CNR for the phase demodulator noise test.

In the experiment, the output noise floor measured on the spectrum analyzer stayed relatively constant for input $CNR_p$ values above 80 dB, as the demodulator noise $N_d$ completely overshadowed the input signal noise $N_i$. The noise floor at this point is the intrinsic demodulator noise itself, measured at $10^{-13}$ W on the spectrum analyzer, in a bandwidth of 10 kHz.

The final step in the derivation is to combine Equations 2.10 and 2.14 to determine the output power $SNR_p$ from the input parameters. Furthermore, for an estimated $CNR_p$ of 64 dB, it reasonable to assume that the demodulator noise $N_d$ can be neglected from Equation 2.14 for the experimental conditions of Chapter three, as explained above with the experimental plot in Figure 2-10.

Hence the relationship between output $SNR_p$ and the input $CNR_p$ reduces to,

$$SNR_p = m_s^2 / (2/CNR_p). \qquad \textbf{(2.15)}$$

The minimum measurable distance is determined by setting $SNR_p$ equal to 1 in Equation 2.15, and computing $m_s$. The result is then converted to an actual displacement using Equations 1.6 and 1.9. For a $CNR_p$ of 64 dB, the result is $44.93 \times 10^{-12}$ m *rms*. Therefore, the expected measurement resolution of the interferometer is 0.04 nm *rms* in a bandwidth of 10 kHz, almost two orders of magnitude smaller than the design goal.

The minimal detectable displacement can be normalized to a bandwidth of 1 Hz by dividing the result computed above by the square root of the bandwidth (see Equations 2.10 and 2.15). This gives a minimal detectable displacement of $449.3 \times 10^{-15}$ m *rms*•$Hz^{05}$.

This is roughly two orders of magnitude larger than the theoretical limit of $10^{-15}$ m•$Hz^{05}$ (Wagner *et al.*, 1987). This discrepancy can be attributed to two factors. Firstly, the *CNR* is maximized when the total optical power incident onto the detector is as large as possible (without saturating the detector) and the internal gain *M* is just barely large enough for shot noise limited detection.

Secondly, the *CNR* is also maximized when the local oscillator power $P_{lo}$ and the signal power $P_s$ incident onto the detector are equal (Waksberg, 1981). Neither condition was satisfied in the experimental conditions of Chapter three.

However, since the resolution requirements for this project were much less demanding than the theoretical limit and since it was expected that the measurements would be mainly limited by environmental noise sources, the objective was simply to achieve shot noise limited detection with a measurement resolution better than 0.1 nm SD (one order of magnitude better than the design goal).

# CHAPTER THREE: NOISE SOURCE ANALYSIS AND EXPERIMENTAL RESULTS

In this chapter, the various noise sources that effect the interferometer (both intrinsic to the device and from the environment) are listed and explained. Whenever possible, their impact on the accuracy of the measurements is estimated.

Then, the results from an experiment are presented where the combined effect of all the noise sources is evaluated. These results demonstrate that the interferometer performance surpasses the high resolution objective of the project by one order of magnitude. The characteristics of the data are related to the noise sources listed in the beginning of the chapter.

Finally, data is presented from an actual practical application experiment where the interferometer was used for precise closed-loop displacement control a non-linear actuator.

## 3.1 Sources of Noise

In this section the various noise sources that originate from the interferometer components and from the environment are listed. Table 3-3, at the end of this section, provides a comparative presentation of all noise sources. The measurement bandwidth for the experiments was 10 kHz, for reasons explained below.

### 3.1.1 Optical Shot Noise

The expected shot noise level for the experiments, as computed is Section 2.4, is $2.137 \times 10^{-12}$ W *rms* for a 10 kHz bandwidth. This corresponds to 44 pm *rms*, as computed from Equations 1.6, 1.9 and 2.15.

### 3.1.2 Demodulator Phase Noise

As explained in Section 2.4, the demodulator electronics have a baseline phase noise $N_d$ which ultimately limits the resolution of the optical phase measurements. This noise was experimentally measured at $10^{-13}$ W *rms* in a bandwidth of 10 kHz. This corresponds to $88 \times 10^{-15}$m *rms* ($k_p$ = 1.8 V/rad) in a bandwidth of 10 kHz, as computed using Equations 1.6, 1.9 and 2.14.

### 3.1.3 Longitudinal Modes

Because of the Doppler broadened gain curve of the He-Ne laser and the long cavity length required for high output power, the laser emits simultaneously on several longitudinal modes (see Figure 3-1). This imposes a spatially periodic modulation on the maximum amplitude of the interference pattern (Foreman, 1967).

For a laser with 4 longitudinal modes such as the one used in the experiments, the spatial modulation period is 0.12 m and the interference term maximum amplitude (see Equation 1.10) decreases by a factor of 100 midway between the peaks.

Hence, care must be taken to ensure that the average path length difference operating point of the interferometer is near a maximum in the modulation pattern. For a path length difference of 10 mm from a peak (the displacement range objective of the design), the maximum amplitude of the interference pattern drops by 10%. As explained in Section 2.2.1, this effect is eliminated by the electronics. It will thus be omitted from the global noise analysis at the end of the section.

### 3.1.4 Source Wavelength Drift

According to the manufacturer, temperature variations in the laser medium

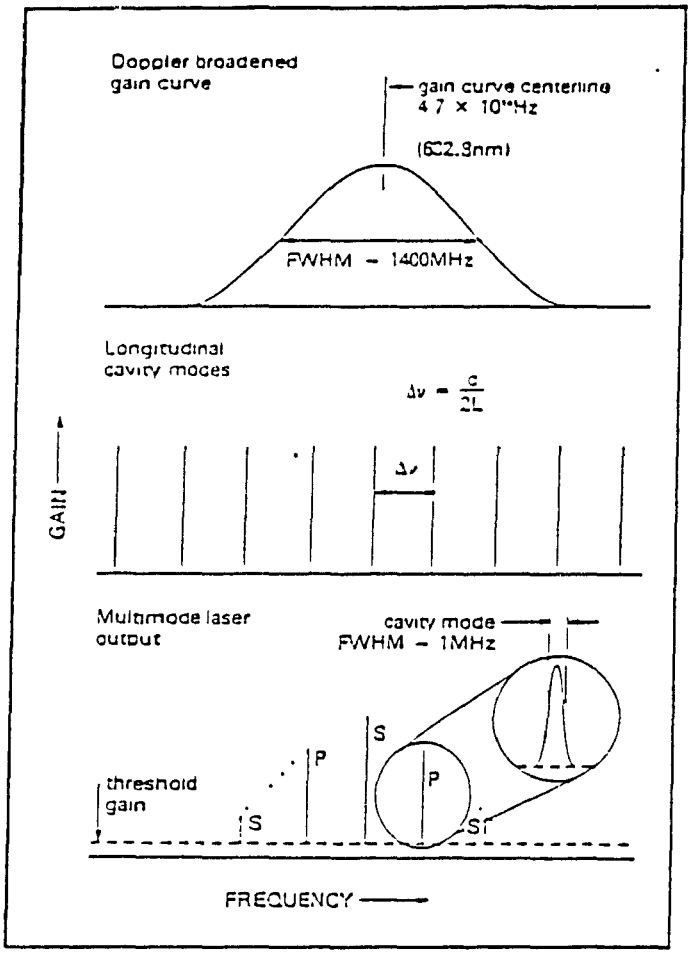


Figure 3-1. Frequency characteristics of a typical Helium-Neon laser (Taken from Melles-Griot, 1988).

cause changes both in the absolute longitudinal mode wavelengths and in the spacing between the modes (known as mode sweeping). Both effects combine to cause appreciable low frequency temperature related variations in the actual laser wavelength, unless the cavity length is actively stabilized.

For research instruments, the vacuum wavelength $\lambda_v$ of the 632.8 nm line of the Helium-Neon laser is stable to $\Delta\lambda/\lambda \sim 10^{-10}$/K, and to $\Delta\lambda/\lambda \sim 10^{-7}$/K for commercially available unstabilized lasers (Bobroff, 1987).

### 3.1.5 Source Power Fluctuations (AM noise)

Fluctuations in the source laser power occur because of relaxation oscillations or shifts in the laser lines with respect to the doppler broadened gain curve (mode sweeping).

However, as explained in Section 2.2.1, the electronics isolate the interferometer from this particular noise source. It will thus be omitted from the global noise analysis at the end of this section.

### 3.1.6 Spatial Mode Beating

Although the Melles-Griot He-Ne laser is designed to emit only in the $TEM_{00}$ mode, in actuality the beam also contains a trace of higher order spatial modes (see Figure 3-2). Because of interactions between the longitudinal and spatial modes, and of non-linearities in the lasing medium, the situation becomes very complex and a number of beat frequencies occur (Eynon *et al.*, 1977). These spurious beat frequencies modulate the phase information in the photo-current from the detector.

This phenomenon was observed experimentally by directing a single laser beam onto a detector and looking at the photo-current on a spectrum analyzer (Avantest model R4136). Under ideal conditions, for a single spatial mode / multi-longitudinal mode laser, one would expect to see a narrow spike in frequency at multiples of $\Delta v$, the longitudinal mode spacing, due to longitudinal mode beating only.

In the experiments however, a spread of frequency components were often observed around the central peaks at $\Delta v$, due to additional spatial mode beating. The frequency spacing between the sidebands appeared to slowly fluctuate over time from near 0 Hz up to ~100 kHz.

A number of lasers were tested and it appeared that the probability of occurrence of the sidebands differed from one particular laser to another. The sidebands appeared almost permanently in the spectrum of a Melles-Griot 10 mW laser, around a few seconds every minute for a 6 mW Newport laser and were virtually unobservable for a 5 mW Hughes laser Hence the problem appeared to be related to the size of the laser cavity.

In the case of the Melles-Griot 10 mW laser, the permanent spatial mode beating was observable at the phase demodulator outputs as a sinusoidal modulation of the output phase signal. The modulation frequency was equal to the sideband spacing observed on the spectrum analyzer and the amplitude was ~150 mVpp. As the output signal from the demodulator is ~4 Vpp, this corresponds to a worst case error of ~4 nm-pp.

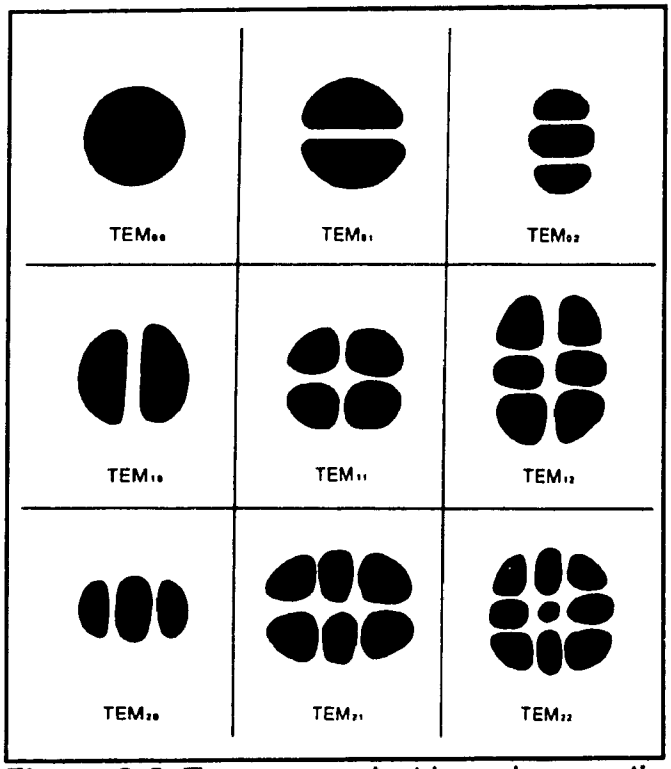


**Figure 3-2.** Transverse electric and magnetic modes of a laser cavity (Taken from Melles-Griot, 1988).

The spatial mode beating noise was a randomly occurring problem, but it was easily recognisable on the spectrum analyzer, so that any data corrupted by it could be discarded. This particular noise source will thus also be omitted from the global noise analysis.

### 3.1.7 Variations in the Index of Refraction of Air

According to Steinmetz *et al.* (1987), the most important source of error in an interferometer is often the change in atmospheric conditions, and the inevitable change in the index of refraction of the ambient air. Table 3-1 lists the variations in environmental parameters (pressure, temperature, humidity and $CO_2$ concentration) required to change the index of refraction of air (and thus the wavelength of light in the medium) by 1 part in $10^6$ (Steinmetz *et al.*, 1987; Estler 1985).

| PARAMETER | REQUIRED CHANGE |
|---|---|
| Temperature | 1°C |
| Pressure | 0.35 kPa |
| Humidity | 80% |
| $CO_2$ Concentration | 67 ppm |

**Table 3-1.** Environment parameter variations which will change the index of refraction of air by $10^{-6}$.

Note that according to Estler (1985), it is very unlikely that variations in $CO_2$ concentrations could be large enough to cause significant errors in interferometer measurements. Note also however that during periods of rapid climatic change such as a passing cold front, the atmospheric pressure may vary by hundreds of Pa (Estler, 1985).

### 3.1.8 Material Size Changes vs Temperature

Due to temperature variations within the enclosure, all of the components in the system will change in size, thus causing unwanted path length changes in the interferometer.

The combined effect of the changing sizes of the various components and different materials is difficult to predict. Table 3-2 lists the coefficients of thermal expansion of the various materials used in the interferometer (Melles-Griot, 1988; Weast *et al.*, 1984), for comparison purposes. Note that Aluminum components will be the most sensitive to thermal shock in the system.

| MATERIAL | COMPONENT | COEFFICIENT OF THERMAL EXPANSION ($x10^{-6}$ / K) |
|---|---|---|
| Aluminum | Mounts | 24.0 |
| Steel | Optical Table Top | 12.1 |
| Ceramics | Mirrors, Lenses | 3.25 |
| Zerodur | Mirrors | 0.1 |

**Table 3-2.** Coefficients of thermal expansion for the various materials used in the interferometer.

As an example, consider Aluminum mirror mounts with a typical base length of 50 mm. If the base is anchored at one end, the opposite end will move by 1.2 μm / K, an enormous amount. The effect of this noise source will be reduced in a future version of the interferometer, described in Chapter 4.

### 3.1.9 Mechanical Vibrations

In a typical laboratory environment, mechanical vibrations originate from two sources: first, from building vibrations at frequencies as low as 2-4 Hz, although most of the vibrational energy is in the 5-30 Hz range (Betzig, 1986); second: from acoustic vibrations in the 20 Hz to 20 kHz range.

The building vibrations are damped by the optical table, and the acoustic vibrations are damped by the vibration isolation cage. The cage is made out of 5 mm thick rigid plastic, padded on the inside with 10 mm thick foam.

### 3.1.10 Comparative Analysis of Noise Sources

In this section, the different noise sources listed above are compared in Table 3-3. Note that the noise sources which affect the laser wavelength are cumulative in that the error increases with the path length difference Hence the worst case error, as presented in the table, occurs at the extreme measurement range (10 mm).

Bandwidth dependent noise sources (shot noise and demodulator noise) are normalized to 10 kHz, the bandwidth in which the experimental measurements presented in the following sections were taken.

| NOISE SOURCE | ERROR MAGNITUDE |
|---|---|
| **Low frequency**: | |
| Laser wavelength drift | 10 nm / K |
| Index of refraction change: | |
| Temperature | 0.1 μm / K |
| Pressure | 0.3 nm / Pa |
| humidity | 1 nm / % change |
| Component thermal expansion | > 1 μm / K |
| Mechanical vibrations (building) | unknown |
| **High frequency**: | |
| Mechanical vibrations (acoustics) | unknown |
| Optical shot noise | 44 pm *rms* (10 kHz BW) |
| Demodulator phase noise | 0 09 pm *rms* (10 kHz BW) |

**Table 3-3** Comparative table of the various interferometer noise sources

It is apparent from Table 3-3 that the dominant sources of error in the interferometer are expect to be the environment noise sources (ambient air, thermal shock).

## 3.2 Experimental Results

Experiments were conducted with the setup shown Figure 2-1. The first set of experiments were aimed at measuring the resting state noise floor in the interferometer (free run measurements) in a 1 second time period, as this is the typical duration of a muscle cell experiment with the micro-robot. In the second set of experiments, the interferometer was used in an actual practical application to demonstrate its usefulness. The results of these experiments are presented in the following sections.

### 3.2.1 Interferometer Resting State (Free Run) Noise Floor

A series of experiments were conducted to evaluate the combined effect of all the noise sources on the interferometer. The objective was to verify that the "High resolution / Low speed" mode design goal of 1 nm *SD* resolution in a 100 kHz bandwidth had been achieved. This Section presents and discusses the experimental data and relates the results to the error analysis above.

The experiments were conducted in a bandwidth of 10 kHz only, as this was the highest sampling rate possible with the available equipment at the time. Note however that the results show that the dominant noise sources in the system are not bandwidth dependant (environmental noise). Hence it is expected that the measurement results can be extended to higher bandwidth with equal resolution

Referring to Figure 2-1, the interferometer was placed into a resting state by the replacing the moving mirror M3 with a fixed mirror. The outputs of the phase demodulator were sampled at high speed for 1 s and the data were then processed by a computer for analysis.

The outputs of the demodulator were anti-aliasing filtered by second-order low-pass 10 kHz cutoff filters, and sampled at 50 kHz by 16 bit A/D converters in a peripheral data acquisition unit (Keithley model 500, with AMM2 master

time on an IBM PC AT and later converted to displacement by the technique explained in Section 2.3. The data were then transferred to a Micro-Vax II computer for data analysis using the NEXUS signal processing software (Hunter and Kearney, 1983). The Quickbasic computer program used to acquire the data for this series of experiments is included in the appendix.

A series of ten such experiments were conducted. The displacement data from a typical experiment are shown in Figure 3-3. The power spectrum and the probability density (corrected for zero mean) of the experimental data are shown in Figures 3-4 and 3-5.

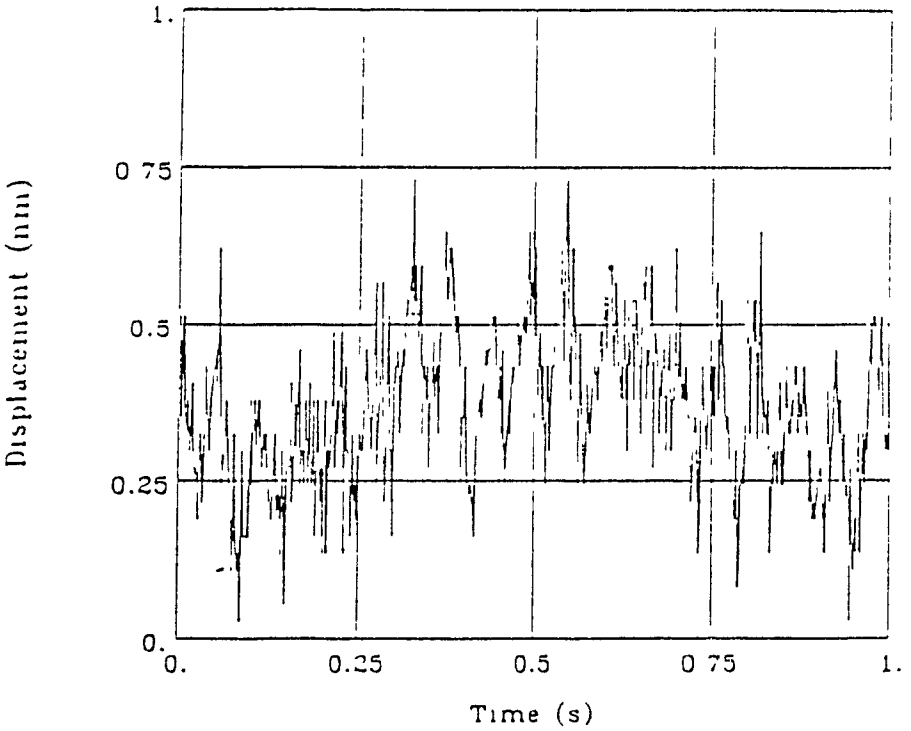


**Figure 3-3.** Plot of typical displacement data versus time from the interferometer in a resting state. The data were sampled at 50 kHz, for 1 s.

The first and most obvious and important result from the experiments, as seen in Figure 3-3, is that the total peak-to-peak noise level of the interferometer

The first and most obvious and important result from the experiments, as seen in Figure 3-3, is that the total peak-to-peak noise level of the interferometer is well below 1 nm, in a bandwidth of 10 kHz. In the probability density plot shown in Figure 3-4, the data (stars) are reasonably fitted as a Gaussian model (solid line). The standard deviation is 0.12 nm, almost one order of magnitude better than the design goal.

Note from Figure 3-5 that the data exhibits a large peak in frequency centred around 400 Hz. This peak is suspected to be a mechanical resonance in the system. This phenomenon was examined in the following qualitative experiment: a metal rod was used to lightly tap the optical table while looking at the outputs of the phase demodulator on a spectrum analyzer. The 400 Hz peak increased by several orders of magnitude at each tap.

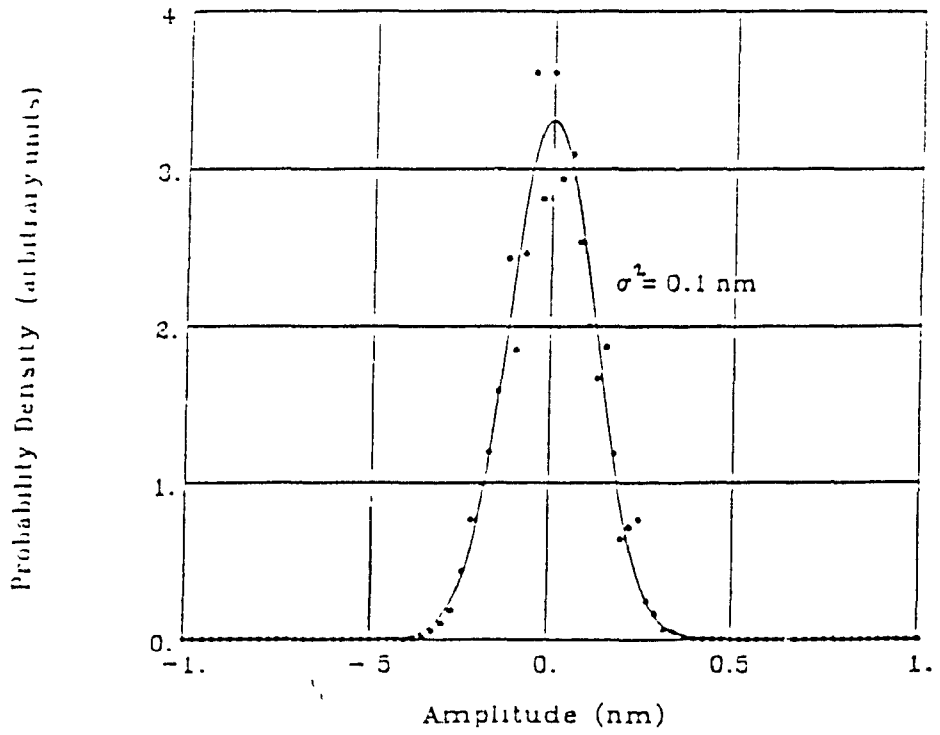


**Figure 3-4.** Plot of the probability density for the typical displacement data from the interferometer in a resting state (points: data, solid curve: Gaussian fit).

Furthermore, an attempt was made to isolate the source of the mechanical resonance by tapping each component in the interferometer separately, and comparing the effects on the spectrum analyzer. Unfortunately, several components appeared to cause an equally powerful resonance, so no specific source could be identified.

It thus appears that the 400 Hz peak is a mechanical resonance due either to the optical table itself, or to a combination of optical components. Any wideband mechanical noise source in the environment will thus cause the interferometer to vibrate at this frequency.

It is also seem from Figure 3-5 that the data exhibit a number of large frequency components below around 30 Hz. These components are the largest in the spectrum. They are probably due to some combination of the low frequency noise factors listed in Table 3-3.

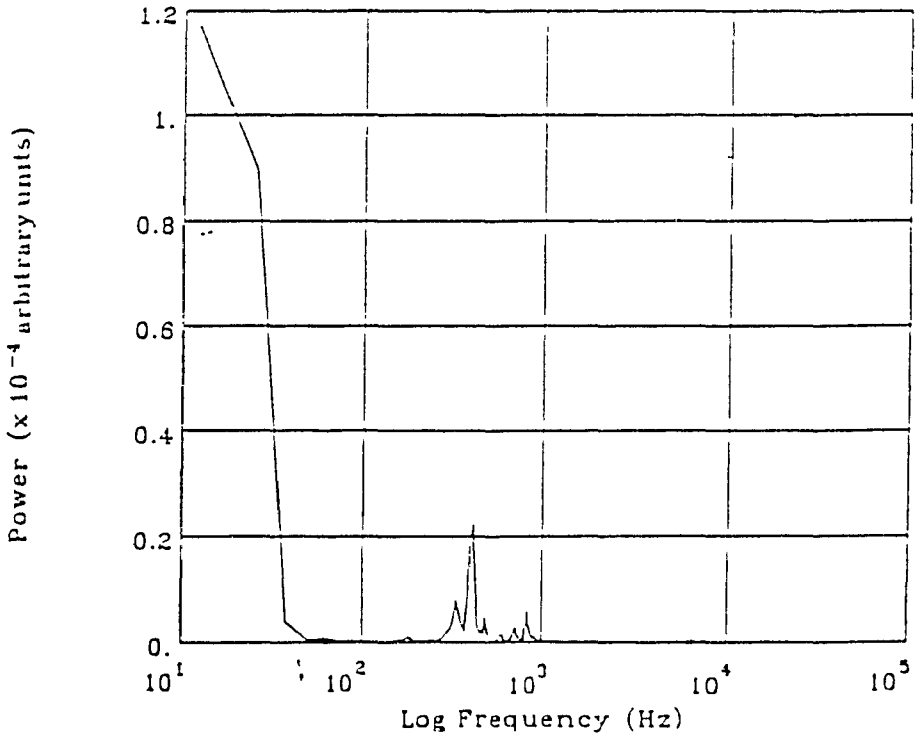


**Figure 3-5.** Plot of the power spectrum for the typical displacement data from the interferometer in a resting state.

The second most important result of the experiments is that by comparing the relative magnitudes of the noise frequency components in Figure 3-5, it is obvious that the dominant noise sources in the system are either due to the environment or to fluctuations in the source laser wavelength (the noise sources are not wideband signals but are sharply peaked in frequency).

The bandwidth dependant noise sources in the system (optical shot noise and demodulator phase noise) are both smaller in magnitude than the environmental noise sources in the experimental data. It is thus expected that if the bandwidth is increased to 100 kHz, the noise floor will remain the same at 0.1 nm *SD*, one order of magnitude better than the design goal.

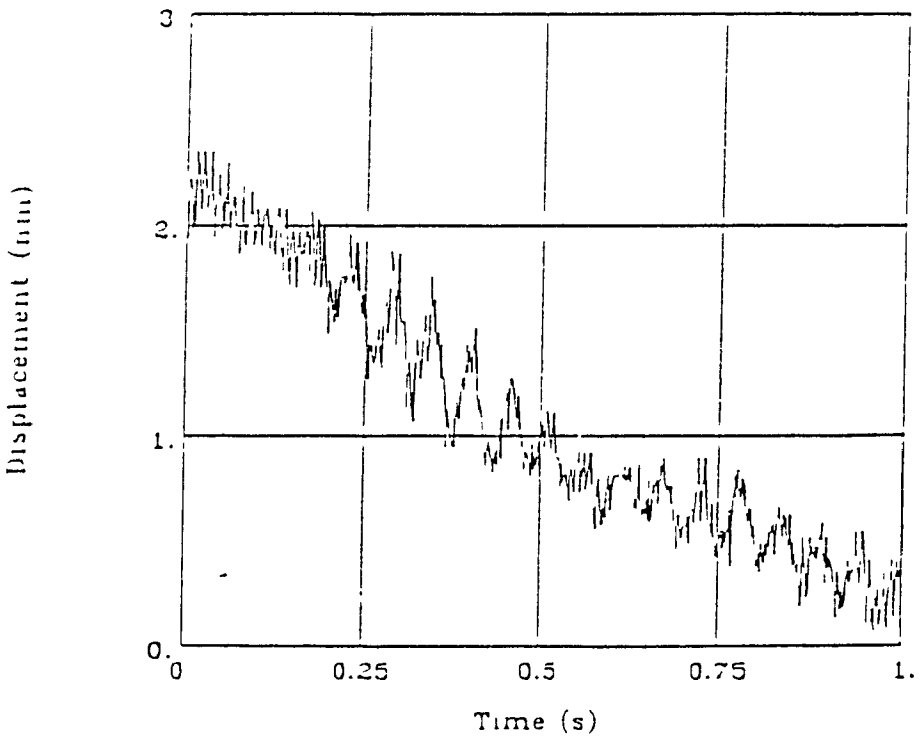


**Figure 3-6.** Interferometer resting state measurements : plot of an atypical data recording versus time where the interferometer was disturbed by some very low frequency perturbation.

Finally, this section also presents additional experimental data which are atypical but frequent enough to be noted in Figure 3-6 In this case, the interferometer has been disturbed by some very low frequency (< 1 Hz) noise source such as a change in the index of refraction of the ambient air or a slow variation in the component temperature. The occurrence probability of this type of effect will be reduced in a future version of the interferometer described in Chapter four.

### 3.2.2 Application to Controlling a Non-Linear Actuator

In this section the results of an experiment are presented where the interferometer was used in the closed-loop control of a non-linear actuator, to demonstrate its practical usefulness.

The actuator under test is the electromagnetic actuator (EMT) shown in Figures 2-1 and 2-2. This solenoid driven displacement device is actuated by applying a control voltage to a driver which supplies the corresponding bias current between the two EMT terminals. The EMT positioning system is capable of open-loop displacement resolution of about 0.1 μm, over a range of 20 μm The relationship between input control voltage and output displacement is non-linear and varies from one device to the next due to the manufacturing process. Hence some form of close-loop control is needed for precise positioning

In the experiment, a proportional control algorithm was implemented in software on the IBM PC AT The Quickbasic computer control program is included in the appendix. The inputs to the program were a desired position command and the actual position as measured by the interferometer using the technique described in Section 2.3. The output of the program was a control voltage to the EMT driver. The control voltage was applied by a 12 bit digital-to-analog converter (D/A).

The EMT was requested under computer control to move over a distance of 0.6 μm, in steps of 25 nm. At each iteration, when the EMT had settled to within 1 nm of the required position, the output voltages from the phase demodulator were recorded in the computer memory. The results of the experiment are plotted in Figure 3-7. Note the quadrature between the two curves.

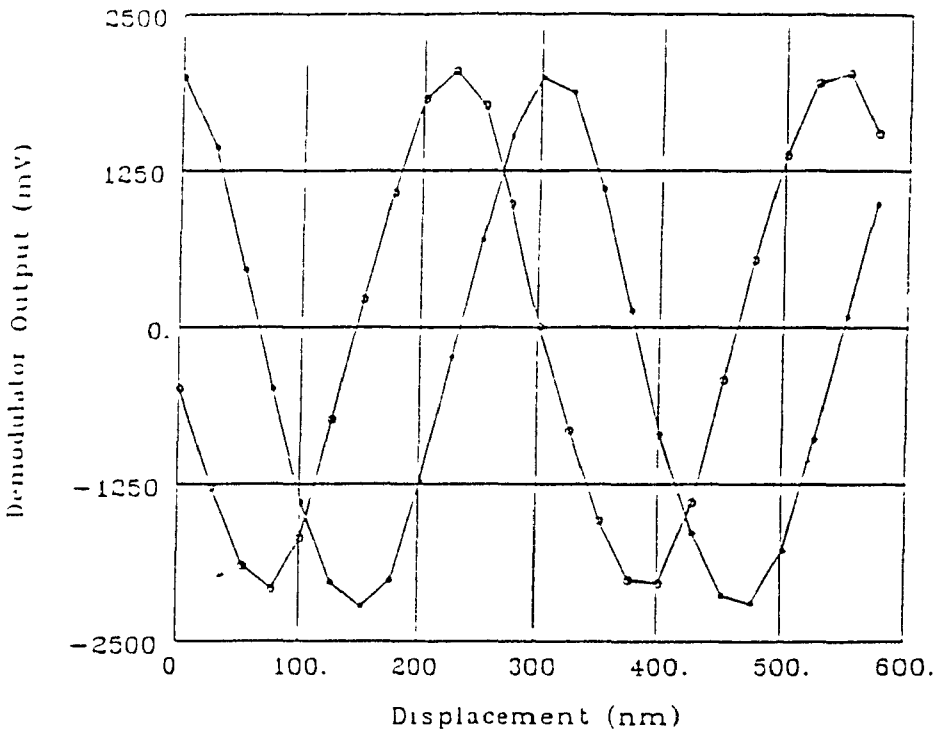


Figure 3-7. Plot of the phase demodulator quadrature output versus displacement for the EMT closed-loop control experiment. (circle markers : sine output, star markers : cosine output)

Finally, it may also be interesting to use the non-linear actuator open loop in certain applications. For this purpose, the data in Figure 3-7 was converted to an input/output characteristic calibration curve for the EMT, as shown in Figure 3-8. Note the non-linearity demonstrated by the I/O curve.

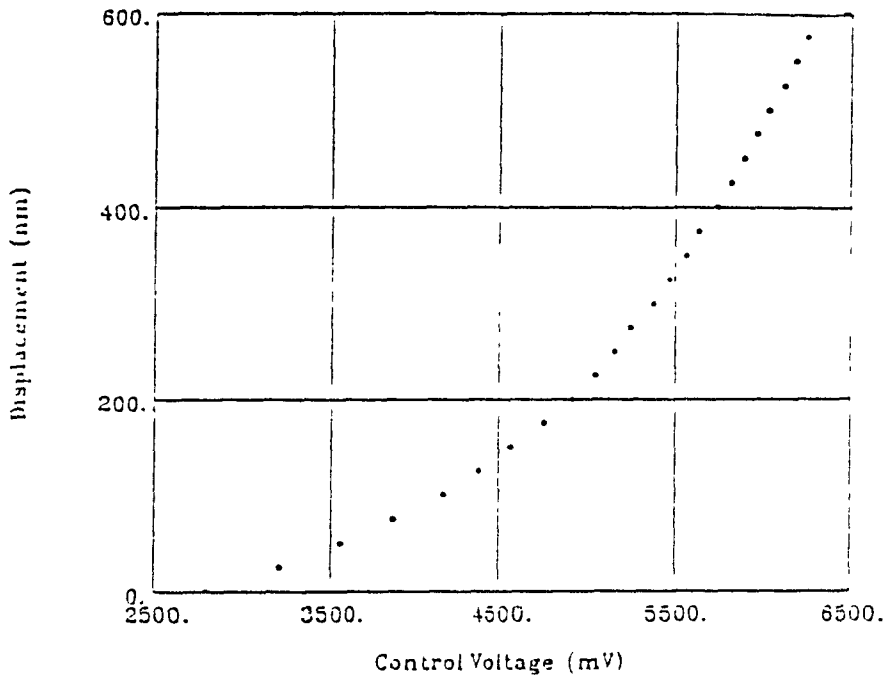


**Figure 3-8.** Plot of the displacement vs control voltage input/output relationship for the EMT.

# CHAPTER 4 :
# IMPROVEMENTS AND FUTURE WORK

In this last chapter, a number of intended improvements to the interferometer design are described. The chapter ends with concluding remarks. The additional work is aimed at reducing the sensitivity of the design to environmental noise and fully integrating the interferometer into the micro-robot system.

## 4.1 Improved Frequency Response of the Electronics

As explained in Section 2.2.2, the frequency response of the electronics could only be determined up to 10 kHz with the present experimental setup. An improved frequency response measurement setup will be devised for characterising the electronics over their full intended working bandwidth of 6 MHz. At this point, the output stage amplifiers (2 MHz bandwidth) will also be replaced with high frequency op-amps (bandwidth > 6 MHz).

## 4.2 Compacting the Optics

As explained in earlier sections, environmental noise sources such as vibrations and thermal shock induce unwanted path length variations in the interferometer. In order to minimize these effects, the total path travelled by the light in the interferometer must be made as short as possible by compacting the device as much as possible.

Furthermore, the micro-robot system is enclosed in a lead-copper-felt cage for vibration and thermal shock isolation. Apart from containing the micro-robot, the cage is densely packed with other assorted equipment. Hence, as a total of six interferometers will be required to measure the robot limb displacements, it is highly desirable that the size of each unit be minimized.

The size of the interferometer will be reduced by eliminating the optical mounts. This will be done by replacing the mirrors with right angle prisms and cementing the optical components together onto a common substrate Also, in order to further reduce the sensitivity of the device to thermal shock, all the optical components will be made out of Zerodur (see Table 3-2).

## 4.3 Interface to the Parallel Computer

Currently, the micro-robot is controlled by a DEC Micro-Vax II computer. The real-time processing requirements of the micro-robot far exceed the capacity of the Micro-Vax II however. For this reason, a novel fully connected parallel computer has been designed in Dr. Hunter's laboratory and is currently being built (Martel *et al.*, 1990).

The interferometer will be required to interface to the parallel computer for data acquisition used in the control of the micro-robot. Each processor in the parallel computer has a I/O subsystem consisting of 16 RS-422 serial I/O 10 Mbit/s channels.

As explained in earlier sections, the interferometer has two modes of operation: "high speed / low accuracy", where fringe counting is sufficient, and "low speed / high accuracy mode", where the full nanometer resolution is required. The requirements for the transmission to the computer of the digitized information in both modes are explained below.

In the high speed mode, the micro-robot limbs can move at speeds up to 2 m/s. This corresponds to a fringe rate of 6.3 million fringes per second. Since only 1 bit is needed to transmit the fringe information, this corresponds to a maximum rate of 6.3 Mbit/s for the "high speed / low accuracy" mode of the interferometer.

In the low speed mode, the 4 Vp-p outputs from the demodulator must be measured with a resolution of 1 mV in order to compute displacements with the

lookup table process described in Section 2.3. Hence, 14 bits are needed to encode the information in the "low speed / high accuracy" mode, at a maximum rate of 100,000 measurements per second. This corresponds to a maximum data rate of 1.4 Mbit/s.

Since the digitization and transmission requirements of both interferometer modes are different, one possible scenario would be to have two A/D converters per demodulator output; one for each mode, with some method to switch under computer control between high speed and low speed modes.

A better method however would involve using only a 1 bit A/D converter per channel and a technique developed by Masry (1981) to recover the high accuracy information from the low accuracy transmitted data. In this technique, white noise with a known probability density is injected into the signal before the digitization, and averaging by the computer restores the original accuracy of the data.

Hence, with this technique, only one mode of operation would be needed, since the data would be continuously transmitted to the computer over 10 Mbit/s RS-422 channels, in 1 bit words. The final accuracy of the displacement computation would depend on the number of averaged measurements by the computer.

## 4.4 Conclusion

In conclusion, recall that the objective of this project was to build a sensor capable of measuring displacements over a range of 10 mm with a resolution of 1 nm *SD* in a bandwidth of 100 kHz, for low speed/high accuracy movements of a micro-robot limb, in a time period of 1 second. The sensor also had to be capable of measuring displacements at high speeds using fringe counting.

It was demonstrated with experimental results that the laser heterodyne interferometer described in this thesis exceeds the design objective by one order

of magnitude in resolution in a bandwidth of 100 kHz. The interferometer was assembled using discrete optical components and included a high frequency electronic circuit for optical phase demodulation. Both the optics and the electronics were experimentally characterized for noise and frequency response. Several software programs were written to control the data acquisition and displacement computation by a computer.

Finally, experimental results concerning an actual practical application were also presented where the interferometer was successfully used in the closed-loop control of a non-linear electromagnetic actuator.

# APPENDIX

- Demodulator Calibration Data Acquisition Program (Sample3.bas)
- Lookup Table Construction Program (MKTable.bas)
- Interferometer Resting State data Acquisition Program (Acquir2.bas)
- EMT Closed-Loop Control Program (Control2.bas)

```
'*****************************************************************
'*
'*       Filename:        Sample3.bas
'*
'*       Created by:      Paul Charette
'*
'*       Last updated:    20 march 1990
'*.
'*       Purpose:         To sample data on analog channels 0,1,2,
'*                        compare the data on 0 to elements of an array
'*                        and when they match, record the data on channels 1,2
'*
'*       Output:          - Sample3.dat : An ASCII file containing the
'*            :           data in millivolts in a BASIC array format.
'*                        - Sample3q.dat . A QUICK500 file containing
'*                        the data in millivolts.
'*
'*****************************************************************

'Initialise hardware
CALL softinit
CALL init

'Declare variables
DIM psbuf!(400)
DIM avbuf1!(400)
DIM avbuf2!(400)

'Initialise screen
SCREEN 0, 0: CLS
LOCATE 3, 16: PRINT "* Phase Demodulator Output Sampling Program *"

' Prompt user for output filenames and comment
PRINT ""
PRINT ""
PRINT ""
PRINT ""
INPUT "Output filename (without extention)"; ofile$
INPUT "Comment"; ocomment$

'Create analog input channels
CALL ionmana("amm20", 1, 0, 16, 1, -1)
CALL ionmana("amm21", 1, 1, 16, 1, -1)
CALL ionmana("amm22", 1, 2, 16, 1, -1)

'Get phase shifter calibration data
CALL arload(new$, "c:\quick500\paul\pscalq.dat")
CALL arstatus(new$, dep!, wid%, lp!, lab$)
CALL argetf(new$, 1, dep, 1, "", psbuf!(), -1)
CALL argel(new$)

'Since the A/Ds can only handle 10v maximum, a voltage divider had to
'be used to sample the voltage on channel 0. Hence the actual voltage
'on channel 0 is is the measured voltage multiplied by the inverse
'of the voltage divider (conversion factor)
'These parameters must be verified with the CAL.BAS program prior to
'making a series of measurements...
cv! = 2.9994
offset! = 3.5
```

```
'Open and initialise the ASCII data file
OPEN "c:\quick500\paul\" + ofile$ + ".dat" FOR OUTPUT AS #1
PRINT #1, "# Phase Demodulator Output Data in mV"
PRINT #1, "# " + ofile$ + "1 is output 1, " + ofile$ + "2 is output 2"
PRINT #1, "# Comment:" + ocomment$
PRINT #1, ""
PRINT #1, ofile$ + "1="
PRINT #1, ofile$ + "2="

'Number of samples for averaging and sampling interval (multiples of 10us)
'    ******  Important note  ******
'Note that a sampling interval of 0 is supposed to select the fastest
'sampling possible  However, voltage readings at this setting are incorrect.
'Furthermore, sampling intervals lower than 5 not only give incorrect readings
'but also cause the PC to fail intermittently (interrupts?).
n! = 100
si% = 15

'Init variables
last0! = 0
last1! = 0
last2! = 0
delta! = 1.9
lsb0inc% = 1
j! = 0
deblag = 0

'Create dummy array for first pass
CALL aning("in012%", n!, "amm20 amm21 amm22", si%, "NT")

'Initialise screen
SCREEN 0, 0: CLS
LOCATE 3, 16: PRINT "* Phase Demodulator Output Sampling Program *"
LOCATE 10, 36: PRINT "[00,10] Volt Interval"

'Zero output voltages on D/As
lsb0% = 0
msb0% = 8
OUT &H711, msb0%
OUT &H710, lsb0%
lsb1% = 0
msb1% = 8
OUT &H713, msb1%
OUT &H712, lsb1%

'Loop all points in the array
FOR i! = 1 TO dep! - 1!
        low! = psbuf!(i!) - delta!
        high! = psbuf!(i!) + delta!
        'Print current voltage interval
        LOCATE 8, 20
        PRINT USING "Sample ### :   #####.#mV , #####.#mV"; i!; low!; high!

        'Loop until sample on channel 0 matches the value in the array...
        DO
                'Increase voltage on phase shifter by one increment
                lsb0% = lsb0% + lsb0inc%
                IF lsb0% > 255 THEN
                        lsb0% = 0
                        msb0% = msb0% + 1
```

```
        END IF
        IF msb0% > 15 THEN
                msb0% = 0
        END IF
        IF (msb0% = 8) AND (lsb0% = 0) THEN
                SELECT CASE msb1%
                CASE 8                          'Go from [0,10]V to [10,20]V
                        lsb1% = 0
                        msb1% = 0
                        delta! = 5.5
                        lsb0inc% = 2
                        LOCATE 10, 36: PRINT "[10,20] Volt Interval"
                CASE 0                          'Go from [10,20]V to [20,30]V
                        lsb1% = 255
                        msb1% = 7
                        delta! = 14!
                        lsb1inc% = 4
                        LOCATE 10, 36: PRINT "[20,30] Volt Interval"
                CASE 7                          'Go from [20,30]V to [0,10]V
                        lsb1% = 0
                        msb1% = 8
                        delta! = 1.9
                        lsb0inc% = 1
                        LOCATE 10, 36: PRINT "[30,10] Volt Interval"
                END SELECT
                OUT &H713, msb1%                'Output to D/A 1
                OUT &H712, lsb1%

                low! = psbuf!(1!) - delta!      'Reset interval
                high! = psbuf!(1!) - delta!     'with new delta!
                LOCATE 8, 20
                PRINT USING "Sample ### :   #####.#mV , #####.#mV"; i!;
        END IF
        OUT &H711, msb0%                        'Output to D/A 0
        OUT &H710, lsb0%

        'Average out n samples at 150 microsecond intervals
        CALL ardel("in012%")
        CALL aninq("in012%", n!, "amm20 amm21 amm22", si%, "NT")
        CALL meandev("in012%", 1, mean!, stdev!, 1!, n!, 1)
        meancor! = (mean! - offset!) * cv!

        'Print mean sampled voltage on screen
        IF depflag = 1 THEN
                LOCATE 10, 25
                PRINT USING "Voltage :   ######.# "; meancor!;
                PRINT "mV"
                INPUT a$
        END IF

LOOP UNTIL ((meancor! >= low!) AND (meancor! <= high!))

'Record the data on channels 1 and 2
CALL meandev("in012%", 2, mean!, stdev!, 1!, n!, 1)
avbuf1!(i!) = mean!
CALL meandev("in012%", 3, mean!, stdev!, 1!, n!, 1)
avbuf2!(i!) = mean!
'PRINT #1, i!, avbuf1!(i!), avbuf1!(i!) - last1!, avbuf2!(i!), avbuf2!(i
PRINT #1, USING ofile$ + "1 = " + ofile$ + "1__######"; avbuf1!(i!)
PRINT #1, USING ofile$ + "2 = " + ofile$ + "2__######"; avbuf2!(i!)
```

```
        j! = j! + 1!
        IF (j! = 50!) THEN      'insert purge statements into vax file...
                j! = 0!
                PRINT #1, "purge/nolog"
        END IF
        last1! = avbuf1!(i!)
        last2! = avbuf2!(i!)
NEXT i!

'Close the data file
CLOSE #1

'Save the data in a QUICK500 file...
CALL armake("dummy!", dep!, -1, "amm21 amm22")
CALL arputf("dummy!", 1!, dep!, -1, "amm21", avbuf1!(), 1)
CALL arputf("dummy!", 1!, dep!, -1, "amm22", avbuf2!(), 1)
CALL arlabel("dummy!", "Phase Demodulator Outputs")
CALL arsave("dummy!", "c:\quick500\paul\" + ofile$ + "q.dat")

'Zero output voltages on D/As
lsb0% = 0
msb0% = 8
OUT &H711, msb0%
OUT &H710, lsb0%
lsb1% = 0
msb1% = 8
OUT &H713, msb1%
OUT &H712, lsb1%

'Plot the data...
SCREEN 1, 0: CLS
LINE (0, 10)-(199, 169), 3, B              'Draw box outline
LINE (1, 11)-(198, 168), 0, BF             'Clear inside of box
LOCATE 1, 2: PRINT "Phase Quadrature Output"
CALL graph("dummy!", "1 2", "1 2", "PAGE0", -2500!, 2500!, "reduce", -1, 1!, dep
LOCATE 23, 1: PRINT "0deg       PHASE       360deg";
LINE (195, 25)-(204, 25), 3
LOCATE 4, 28: PRINT "+2 Volts"
LINE (195, 90)-(204, 90), 3
LOCATE 12, 28: PRINT " 0 Volts"
LINE (195, 155)-(204, 155), 3
LOCATE 20, 28: PRINT "-2 Volts"

'Wait for user to press a key to return to alpha mode...
LOCATE 25, 1: INPUT "Press <Cr> to terminate...", a$
CALL ardel("dummy!")
```

```
DECLARE FUNCTION acos! (x!)
DECLARE FUNCTION asin! (x!)
DECLARE SUB FillCol (c1%)
'*************************************************************************
'*
'*       Filename:        MkTable.bas
'*
'*       Created by:      Paul Charette
'*
'*       Last updated:    13 April 1990
'*
'*       Purpose:         Build lookup table
'*
'*       Output:          Lookup table
'*
'*************************************************************************

'Initialise hardware
CALL softinit
CALL init

'Basic random access file record format
TYPE recordtype
        a11 AS INTEGER
        a12 AS INTEGER
        a21 AS INTEGER
        a22 AS INTEGER
        w   AS INTEGER
END TYPE
DIM recordvar AS recordtype

'Create storage
DIM SHARED tlen%
tlen% = 5000

DIM SHARED table%(5, tlen%)
DIM barn1!(720)
DIM barn2!(720)

'Create analog input channels
CALL ionmana("amm20", 1, 0, 16, 1, -1)
CALL ionmana("amm21", 1, 1, 16, 1, -1)
CALL ionmana("amm22", 1, 2, 16, 1, -1)

'Initialise screen
SCREEN 0, 0: CLS
LOCATE 1, 20: PRINT "Lookup table creation program"

'Load the QUICK500 file containing calibration curves
LOCATE 3, 10: INPUT "QUICKBASIC file name (without extention)"; ifname$
CALL arload(infile$, "c:\quick500\paul\" + ifname$ + "q.dat")
CALL arstatus(infile$, dep!, wid%, lp!, lab$)
CALL argetf(infile$, 1!, dep!, -1, "amm21", barn1!(), 1)
CALL argetf(infile$, 1!, dep!, -1, "amm22", barn2!(), 1)
LOCATE 4, 10: PRINT "Information in file [ " + ifname$ + "q.dat ] loaded."

'WRAP AROUND PROBLEMS:
'       If the beginning of the LUT corresponds to any multiple of 90
'degrees, either channel will have a large uncertainty at the edge of the
'LUT. Although the weight will be low, one of the entries of the lut will
```

```
'oscillate between 0 and 360 degrees. This will cause problems...
'In order to eliminate wrap around problems, the calibartion data may
'need to be "rotated" so that the beginning of the array (and hence the end)
'corresponds to an angle for which both the SIN and COS have sharp slopes
'(ex: 45 degrees). This will not affect the distance measurements, as they
'are relative to each other.
'
'However, the problem might still occur. To check for this, both angles
'found in the lookup table must be compared. If they differ by more than
'some threshold value, an error flag should be raised...
'
'Method:
'       Attempt to estimate the angle corresponding to the first data pair
'in the calibration array. Use this angle to determine the necessary rotation
'in the array so that the first pair now correspond to a 45 degree phase
'difference.
'
'Also: use the knowledge of the approximate phase angle to assign weights
'to the data pairs, using SIN and COS. Note that the instantaneous slope
'of the calibration data could be used, but since error in these measurements
'already exist, this would be like compounding the error.
'
LOCATE 6, 10: PRINT "Rotating calibration data to 45 degree multiple..."
'Find maximum amplitude in calibration data, to normalise for computation
'of ASIN and ACOS...
maxamp! = 0!
FOR i% = 1 TO 400
        IF (ABS(barn1!(i%)) > maxamp!) THEN
                maxamp! = ABS(barn1!(i%))
        END IF
        IF (ABS(barn2!(i%)) > maxamp!) THEN
                maxamp! = ABS(barn2!(i%))
        END IF
NEXT i%
LOCATE 7, 15: PRINT "Maximum amplitude: ", maxamp!, " mV"

'Rotate calibration data by extending the array and starting off
'at the location of the approximate location of the 45 degree pair
FOR i% = 1 TO 360
        barn1!(i% + 360) = barn1!(i%)
        barn2!(i% + 360) = barn2!(i%)
NEXT i%

i45% = 1
DO
        i45% = i45% + 1
LOOP UNTIL ((barn1!(i45%) > 0!) AND (ABS(barn1!(i45%) - barn2!(i45%)) < 50!))
LOCATE 8, 15. PRINT "Approximate position of 45 degree entry: ", i45%

'Lookup table structure:
'
'                    Channel1          Channel2
'
'                 /  ------------  \ /  ------------  \
'
'                  Angle11 Angle12 Angle21 Angle22 Weight
'                  ---------------------------------------
'        25000mV  |       |       |       |       |       |
'                 .       .       .       .       .       .
'                 .       .       .       .       .       .
```

```
'            0mV |       |       |       |       |       |
'                .       .       .       .       .       .
'                .       .       .       .       .       .
'     - 25000mV |       |       |       |       |       |
'               ----------------------------------------
'
'Channel1 and Channel2 are the two outputs of the phase demodulator.They are
'roughly proportional to the sine and cosine of the phase angle
'between the signal and the reference inputs to the demodulator, and
'they are approximately in quadrature. The first three columns correspond
'to the calibration data for channel 1 and the last three columns
'to the calibration data for channel 2.
'
'For any given value of voltage, there will be two possible corresponding
'phase angles (sine and cosine are not single valued functions). If the
'voltage on both channels is of the same polarity, then angle1 is the correct
'angle. If the voltages are of opposite polarity, then angle2 is the correct
'angle. The weight is the instantaneous slopes on the output curves.
'It is used to distribute the relative uncertainty between the two
'measured channel voltages.
'
'The table is filled in the following manner: during the calibration
'process, output voltages are recorded for phase shifts from 0 to 360 degrees
'inclusively. These phase angles are inserted at the corresponding voltages
'in the table, according to the principle described above. The blanks between
'known voltage values are filled with the values from the closest upper and
'lower known values.
'
'The actual position computation will look something like this:
'
'       IF (Channel 1 voltage) "same sign as" (Channel 2 voltage)
'                THEN
'                        (
'                        A1 = Table(Voltage1, Angle11)
'                        A2 = Table(Voltage2, Angle21)
'                        )
'                ELSE
'                        (
'                        A1 = Table(Voltage1, Angle12)
'                        A2 = Table(Voltage2, Angle22)
'                        )
'
'                W1 = Table(Voltage1, Weight)
'                W2 = Table(Voltage2, Weight)
'
'                ANGLE = ( (A1 * W1) + (A2 * W2) ) / (W1 + W2)
'
'                POSITION = (ANGLE / 360) * (632.8nm / 2)
'
'First pass on the table where the known voltages are filled in
LOCATE 10, 10: PRINT "First pass on the lookup table..."

'Fill table with dummy value
FOR i% = 1 TO 5
        FOR j% = 1 TO tlen%
                table%(i%, j%) = -1
        NEXT j%
NEXT i%

'Loop for first pass to enter known angles and weights into the table...
```

```
w% = 5
angle% = 1

FOR i% = i45% TO i45% + 359
        index1! = barn1!(i%)
        index2! = barn2!(i%)

        'Check for correct angle column
        IF (((index1! >= 0!) AND (index2! >= 0!)) OR ((index1! < 0!) AND (index2
                A1% = 1
                A2% = 3
        ELSE
                A1% = 2
                A2% = 4
        END IF

        'Store angles into the table...
        table%(A1%, INT(index1!) + (tlen% / 2)) = angle%
        table%(A2%, INT(index2!) + (tlen% / 2)) = angle%

        'Store weights into the table...
        windex% = INT(maxamp! * SIN(angle% * 3.14159 / 180!)) + (tlen% / 2)
        weight! = COS(angle% * 3.14159 / 180!)
        table%(w%, windex%) = INT(weight! * weight! * 50)

        'Increment angle counter...
        angle% = angle% + 1
NEXT i%

'Second pass on the table where the blanks are filled in...
LOCATE 11, 10: PRINT "Second pass on the lookup table..."

LOCATE 12, 15: PRINT "Column 1..."
CALL FillCol(1)
LOCATE 13, 15: PRINT "Column 2..."
CALL FillCol(2)
LOCATE 14, 15: PRINT "Column 3..."
CALL FillCol(3)
LOCATE 15, 15: PRINT "Column 4..."
CALL FillCol(4)
LOCATE 16, 15: PRINT "Column 5..."
CALL FillCol(5)

'Save lookup table in a binary file
LOCATE 17, 10: PRINT "Saving lookup table to disk..."
OPEN "c:\quick500\paul\" + ifname$ + "b.lut" FOR RANDOM AS #1 LEN = LEN(recordva
FOR i% = 1 TO tlen%
        recordvar.a11 = table%(1, i%)
        recordvar.a12 = table%(2, i%)
        recordvar.a21 = table%(3, i%)
        recordvar.a22 = table%(4, i%)
        recordvar.w = table%(5, i%)
        PUT #1, i%, recordvar
NEXT i%
CLOSE #1

'Retrieve the data from the binary file and store it in the ASCII file...
OPEN "c:\quick500\paul\" + ifname$ + ".lut" FOR OUTPUT AS #2
OPEN "c:\quick500\paul\" + ifname$ + "b.lut" FOR RANDOM AS #1 LEN = LEN(recordva
FOR i% = 1 TO tlen%
```

```
        GET #1, i%, recordvar
        PRINT #2, i% - (tlen% / 2), recordvar.all, recordvar.all, recordvar.all,
NEXT i%
CLOSE #1
CLOSE #2

'Wait for user to exit...
BEEP
LOCATE 23, 10: PRINT "Hit any key to return to DOS..."
WHILE INKEY$ = ""
WEND


FUNCTION acos! (x!)
        IF x! = 0 THEN
                x! = .000001
        END IF
        yrads! = ATN(SQR(1 - (x! * x!)) / x!)
        IF (yrads! < 0) THEN
                acos! = (yrads! / 3.141593 * 180!) - 180!
        ELSE
                acos! = (yrads! / 3.141593 * 180!)
        END IF
END FUNCTION

FUNCTION asin! (x!)
        IF x! = 1! THEN
                x! = .99999
        END IF
        IF x! = -1! THEN
                x! = -.99999
        END IF
        yrads! = ATN(x! / SQR(1 - (x! * x!)))
        asin! = yrads! / 3.141593 * 180!
END FUNCTION

SUB FillCol (c1%)
i% = 1
DO
        lalfill% = table%(c1%, i%)      'Record last known value

        j% = i%                         'Find next known value
        DO
                j% = j% + 1
        LOOP UNTIL ((table%(c1%, j%) <> -1) OR (j% = tlen%) OR (j% = (tlen% / 2)

        runt% = j% - i% - 1             'Distance between pairs

        IF (runt% = 0) THEN             'No gap, loop for more...
                i% = i% + 1

        ELSEIF (j% = (tlen% / 2)) THEN  'Zero crossing...
                FOR k% = i% + 1 TO j% - 1
                        table%(c1%, k%) = lalfill%
                NEXT k%
                i% = j%

        ELSEIF (lalfill% = -1) THEN     'Bot of table, fill it in reverse...
                lalfill% = table%(c1%, j%)
```

```
                FOR k% = i% TO j% - 1
                        table%(c1%, k%) = halffill%
                NEXT k%
                i% = j%

        ELSEIF (j% = tlen%) THEN        'Top of table, fill it and stop
                FOR k% = i% + 1 TO tlen%
                        table%(c1%, k%) = halffill%
                NEXT k%
                i% = tlen%
        ELSE                            'Fill in gap between two known pairs
                hrunt% = runt% / 2
                IF hrunt% > 0 THEN
                        FOR k% = i% - 1 TO i% + hrunt%  'First half...
                                table%(c1%, k%) = halffill%
                        NEXT k%
                END IF
                halffill% = table%(c1%, j%)
                FOR k% = i% + hrunt% + 1 TO j% - 1      'Second half...
                        table%(c1%, k%) = halffill%
                NEXT k%
                i% = j%
        END IF
LOOP UNTIL i% = tlen%


END SUB
```

```
'*********************************************************************
'*
'*       Filename:       Acquir2.bas
'*
'*       Created by:     Paul Charette
'*
'*       Last updated:   9 April 1990
'*
'*       Purpose:        Acquire data on channel 0
'*
'*       Output:         ASCII file
'*
'*********************************************************************

'Initialise hardware
CALL softinit
CALL init

'Initialise screen
SCREEN 0, 0: CLS
LOCATE 1, 20: PRINT "Data Acquisition on Channel 0"

'Create analog input channels
CALL ionmana("amm20", 1, 0, 16, 1, -1)

'Get output data filename, comment and number of samples to take...
LOCATE 4, 10: INPUT "ASCII output file name (without extention)"; ofile$
LOCATE 5, 10: INPUT "Comment"; ocomment$
LOCATE 7, 10: INPUT "Number of samples"; n!

'Open and initialise the ASCII data file
OPEN "c:\quick500\paul\" + ofile$ + ".dat" FOR OUTPUT AS #1
PRINT #1, "= Phase Demodulator Output Data in mV"
PRINT #1, "# Comment:" + ocomment$
PRINT #1, ""
PRINT #1, "Number of samples     :"; n!
PRINT #1, "Sampling frequency    : 50KHz"
PRINT #1, "Anti-aliasing filter : 20KHz"
PRINT #1, ""
PRINT #1, ofile$ + "1="

'Compute sub-array size
sn! = INT(n! / 5) + 1

'Create variables
DIM barn1!(sn!)
DIM barn2!(sn!)
DIM barn3!(sn!)
DIM barn4!(sn!)
DIM barn5!(sn!)

LOCATE 10, 10: PRINT "Data acquisition on channel 0 in progress..."
CALL aninq("in0%", sn!, "amm20 amm20 amm20 amm20 amm20", 0, "NT")
CALL argetf("in0%", 1!, sn!, 1, "", barn1!(), 1)
CALL argetf("in0%", 1!, sn!, 2, "", barn2!(), 1)
CALL argetf("in0%", 1!, sn!, 3, "", barn3!(), 1)
CALL argetf("in0%", 1!, sn!, 4, "", barn4!(), 1)
CALL argetf("in0%", 1!, sn!, 5, "", barn5!(), 1)
CALL ardel("in0%")
LOCATE 11, 10: PRINT "Data acquisition on channel 0 done."
```

```
'Find min and maximum values of data
LOCATE 14, 10: PRINT "Computing data extrema..."
max0! = -10000!
min0! = 10000!
FOR i! = 1 TO sn!
        IF barn1!(i!) < min0! THEN min0! = barn1!(i!)
        IF barn1!(i!) > max0! THEN max0! = barn1!(i!)
        IF barn2!(i!) < min0! THEN min0! = barn2!(i!)
        IF barn2!(i!) > max0! THEN max0! = barn2!(i!)
        IF barn3!(i!) < min0! THEN min0! = barn3!(i!)
        IF barn3!(i!) > max0! THEN max0! = barn3!(i!)
        IF barn4!(i!) < min0! THEN min0! = barn4!(i!)
        IF barn4!(i!) > max0! THEN max0! = barn4!(i!)
        IF barn5!(i!) < min0! THEN min0! = barn5!(i!)
        IF barn5!(i!) > max0! THEN max0! = barn5!(i!)
NEXT i!
LOCATE 15, 15: PRINT "Maximum value:     "; max0!; " mV"
LOCATE 16, 15: PRINT "Minimum value:     "; min0!; " mV"
LOCATE 17, 15: PRINT "Maximum excursion: "; max0! - min0!; " mV"

'Write channel 0 data
LOCATE 20, 10: PRINT "Writing channel 0 data to file..."
j! = 0
LOCATE 21, 15: PRINT "Channel 0, Element "; 0!
FOR i! = 1 TO sn!
        IF (j! = 50!) THEN  'Insert purge statements into vax file...
                j! = 0!
                PRINT #1, ".purge/nolog"
                LOCATE 21, 15: PRINT "Channel 0, Element "; INT(i! - 1!) * 5
        END IF
        j! = j! + 1!

        PRINT #1, ofile$ + "1 = " + ofile$ + "1";
        PRINT #1, USING "__######__######__######__######__######"; barn1!(i!);
NEXT i!
LOCATE 21, 15: PRINT "Channel 0, Done.          "

CLOSE #1

'Wait for user to exit...
BEEP
LOCATE 23, 10: PRINT "Hit any key to return to DOS..."
WHILE INKEY$ = ""
WEND
```

```
DECLARE FUNCTION SamplePos! (v1!, v2!)
DECLARE SUB VoltsOut (vin!)
'*********************************************************************
'*
'*       Filename:        Control2.bas
'*
'*       Created by:      Paul Charette
'*
'*       Last updated:    3 may 1990
'*
'*       Purpose:         To move the EMT under computer control,
'*                        in steps of 25 nanometers. At each step, the
'*                        control voltage to the EMT is recorded.
'*
'*                        The program plots the position of the EMT
'*                        in real time, against a plot of the ideal step
'*                        trajectory, in increments of 5 nanometers.
'*                        Finally, the program plots the control voltage
'*                        versus position relationship of the EMT.
'*
'*       Output:          Not'in
'*
'*********************************************************************

'Initialise hardware
CALL softinit
CALL init

'Declare variables
TYPE recordtype
        a11 AS INTEGER
        a12 AS INTEGER
        a21 AS INTEGER
        a22 AS INTEGER
        w   AS INTEGER
END TYPE
DIM recordvar AS recordtype

'Create storage
DIM VoltsRec!(100)
DIM InRec!(100, 2)
DIM PosRec!(100)

DIM SHARED tlen%
tlen% = 5000
DIM SHARED table%(5, tlen%)
DIM PemtRec!(2000)

'Initialise variables
DIM SHARED PosOffset!
PosOffset! = 0!
DIM SHARED LastTheta!
LastTheta! = 0
DIM SHARED fc%
fc% = 0
NSteps! = 25!
Gain! = 2
VOp! = 600!
CALL VoltsOut(VOp!)
```

```
'Create analog input channels
CALL ionmana("amm20", 1, 0, 16, 1, -1)
CALL ionmana("amm21", 1, 1, 16, 1, -1)
CALL ionmana("amm22", 1, 2, 16, 1, -1)

'Initialise screen
SCREEN 0, 0: CLS
LOCATE 1, 20: PRINT "* EMT Control Loop *"

'Load the lookup table
ifname$ = "file4"
LOCATE 3, 10: PRINT "Loading Lookup Table..."
OPEN "c:\quick500\paul\" + ifname$ + "b.lut" FOR RANDOM AS #1 LEN = LEN(recordva
RedFact% = (5000 - tlen%) / 2
FOR i% = (RedFact% + 1) TO (tlen% - RedFact%)
        GET #1, i%, recordvar
        table%(1, i%) = recordvar.a11
        table%(2, i%) = recordvar.a12
        table%(3, i%) = recordvar.a21
        table%(4, i%) = recordvar.a22
        table%(5, i%) = recordvar.w
NEXT i%
CLOSE #1
LOCATE 3, 10: PRINT "Lookup table loaded.      "

'Open ASCII output files
OPEN "c:\quick500\paul\contr2a.dat" FOR OUTPUT AS #2
PRINT #2, "# Phase demodulator output #1"
OPEN "c:\quick500\paul\contr2b.dat" FOR OUTPUT AS #3
PRINT #3, "# Phase demodulator output #2"
OPEN "c:\quick500\paul\contr2c.dat" FOR OUTPUT AS #4
PRINT #4, "# EMT control voltage for 25nm steps"

'Set up screen
SCREEN 1
CLS
LINE (30, 160)-(30, 1), 1
LINE (18, 151)-(318, 151), 1
LINE (28, 127)-(32, 127), 1
LINE (28, 107)-(32, 107), 1
LINE (28, 87)-(32, 87), 1
LINE (28, 67)-(32, 67), 1
LINE (28, 47)-(32, 47), 1
LINE (28, 27)-(32, 27), 1
LINE (28, 7)-(32, 7), 1
LOCATE 14, 1: PRINT "200"
LOCATE 9, 1: PRINT "400"
LOCATE 4, 1: PRINT "600"
LOCATE 1, 2: PRINT "nM"
LOCATE 21, 30: PRINT "Time"
LOCATE 23, 2: PRINT "Closed Loop EMT Control (25 nM Steps)"

FOR i! = 2! TO 25!
        LINE (8! + (i! * 12!), 152! - (i! * 5!))-(20! + (i! * 12!), 152! - (i! *
        LINE (20! + (i! * 12!), 152! - (i! * 5!))-(20! + (i! * 12!), 147! - (i!
NEXT i!

j% = 32
k% = 1
FOR Pref! = 50! TO (25! * NSteps!) STEP 25!
```

```
        FOR i! = 1 TO 12!
                'Sample position
                CALL aninq("in01%", 2!, "amm20 amm21", 0, "NT")
                CALL argetvalf("in01%", 2!, 1, "", v1!, 1)
                CALL argetvalf("in01%", 2!, 2, "", v2!, 1)
                CALL ardel("in01%")
                Pemt! = SamplePos!(v1!, v2!)

                'Compute error signal
                es! = Pref! - Pemt!

                'Output voltage signal to EMT
                Vout! = VOp! + (Gain! * es!)
                CALL VoltsOut(Vout!)
                VOp! = Vout!

                'Plot the pixel
                LOCATE 3, 8: PRINT USING "Position :#### nM"; Pemt!
                PSET (j%, 152 - INT(Pemt! / 5!))
                j% = j% + 1
        NEXT i!
        VoltsRec!(k%) = (Vout! * 4.45) - 300!
        PRINT #2, v1!
        PRINT #3, v2!
        PRINT #4, VoltsRec!(k%)
        PosRec!(k%) = Pemt!
        k% = k% + 1
NEXT Pref!

'Close ASCII FIles
CLOSE #2
CLOSE #3
CLOSE #4

'Wait for user prompt
LOCATE 24, 1: PRINT " Press any key to continue...";
WHILE INKEY$ = ""
WEND

'Plot Position versus Voltage curve
CLS
LINE (30, 160)-(30, 1), 1
LINE (18, 151)-(318, 151), 1
LINE (28, 128)-(32, 128), 1
LINE (28, 108)-(32, 108), 1
LINE (28, 88)-(32, 88), 1
LINE (28, 68)-(32, 68), 1
LINE (28, 48)-(32, 48), 1
LINE (28, 28)-(32, 28), 1
LINE (28, 8)-(32, 8), 1
LOCATE 14, 1: PRINT "200"
LOCATE 9, 1: PRINT "400"
LOCATE 4, 1: PRINT "600"
LOCATE 1, 2: PRINT "nM"
LOCATE 23, 8: PRINT "EMT Motion vs Control Voltage"

vo! = VoltsRec!(1)
v1! = VoltsRec!(NSteps! - 2)
LOCATE 21, 2: PRINT USING "   ####              mV              ####"; vo!; v1!
Vcf! = (v1! - vo!) / 280!
```

```
FOR k% = 1 TO NSteps - 2
        PSET (30 + INT((VoltsRec!(k%) - vo!) / Vcf!), 151 - INT(PosRec!(k%) / 5!
NEXT k%


'*********************************************************************
'*
'*      Function name:  SamplePos
'*
'*      Created by:     Paul Charette
'*
'*      Last updated:   17 April 1990
'*
'*      Purpose:        To sample data on analog channels 0,1
'*                      and compute the new position using the lookup table
'*
'*      Returns:        New Position in NanoMeters
'*
'*********************************************************************
FUNCTION SamplePos! (v1!, v2!)
'The actual position computation will look something like this:
'
'       IF (Channel 1 voltage) "same sign as" (Channel 2 voltage)
'               THEN
'                       (
'                       A1 = Table(Voltage1, Angle11)
'                       A2 = Table(Voltage2, Angle21)
'                       )
'               ELSE
'                       (
'                       A1 = Table(Voltage1, Angle12)
'                       A2 = Table(Voltage2, Angle22)
'                       )
'
'               W1 = Table(Voltage1, Weight)
'               W2 = Table(Voltage2, Weight)
'
'               ANGLE = ( (A1 * W1) + (A2 * W2) ) / (W1 + W2)
'
'               POSITION = (ANGLE / 360) * (632.8nm / 2)
'

'Use sampled voltages on both channels to compute indexes
i1% = INT(v1!) + tlen% / 2
i2% = INT(v2!) + tlen% / 2
'LOCATE 5, 10: PRINT USING "I1:#####  I2:#####  V1:#####  V2:#####"; i1%; i2%; v

'Compute actual angle using weighted function of both measured voltages...
IF (((v1! >= 0!) AND (v2! >= 0!)) OR ((v1! < 0!) AND (v2! < 0!))) THEN
        a1% = table%(1, i1%)
        a2% = table%(3, i2%)
ELSE
        a1% = table%(2, i1%)
        a2% = table%(4, i2%)
END IF
w1% = table%(5, i1%)
w2% = table%(5, i2%)

IF (ABS(a1% - a2%) < 90) THEN
        'Normal case...
```

```
        theta! = ((a1% * w1%) + (a2% * w2%)) / (w1%.+ w2%)
ELSE
        'Check for jumps in the lut...
        theta! = a1%
END IF
RelPos! = (theta! / 360!) * 316.4
'LOCATE 6, 10: PRINT USING "A1:#####  A2:#####  W1:#####  W2:#####  THETA:####.#

'Check for 360 degree jump...
IF (ABS(LastTheta! - theta!) > 180!) THEN
        IF (theta! > LastTheta!) THEN
                PosOffset! = PosOffset! - 316.4
                fc% = fc% - 1
        ELSE
                PosOffset! = PosOffset! + 316.4
                fc% = fc% + 1
        END IF
END IF
NewPos! = PosOffset! + RelPos!
'LOCATE 7, 10: PRINT USING "Theta:#####  LastTheta:#####  RelPos:#####  NewPos:#

'Return position
LastTheta! = theta!
SamplePos! = NewPos!

END FUNCTION

'*********************************************************************
'*
'*      Function name:  VoltsOut
'*
'*      Created by:     Paul Charette
'*
'*      Last updated:   18 April 1990
'*
'*      Purpose:        To output a voltage (in mV) on D/A channel 0
'*
'*      Returns:        Not'in
'*
'*********************************************************************
SUB VoltsOut (vin!)
        twoscomp% = INT((4096! * vin! / 5000!) - 2048!)
        low% = INT(twoscomp% / 256!)
        OUT &H711, low%
        OUT &H710, twoscomp% - (256 * low%)
END SUB
```

```
'*****************************************************************
'*
'*       Filename:       Util.bas
'*
'*       Created by:     Paul Charette
'*
'*       Last updated:   13 march 1990
'*
'*       Purpose:        Stuff
'*
'*       Output:         None
'*
'*****************************************************************

'Initialise hardware
CALL softinit
CALL init

'Declare variables
DIM psbuf!(400)
DIM newbuf!(400)
DIM avbuf2!(400)

'Initialise screen
SCREEN 0, 0: CLS

'Create analog input channels
CALL ionmana("amm20", 1, 0, 16, 1, -1)
CALL ionmana("amm21", 1, 1, 16, 1, -1)
CALL ionmana("amm22", 1, 2, 16, 1, -1)

n! = 100
si% = 15
cv! = 2.999

WHILE 1 = 1
        CALL aninq("in012%", n!, "amm20 amm21 amm22", si%, "NT")
        CALL meandev("in012%", 1, mean!, stdev!, 1., n!, 1)
        CALL ardel("in012%")
        meancor! = mean! * cv!

        'Print mean sampled voltage on screen
        LOCATE 10, 25
        PRINT USING "Voltage :   ######.# "; meancor!;
        PRINT "mV"

        'Input desired voltage...
        LOCATE 5, 25
        INPUT "MSB1,LSB1,MSB0,LSB0"; msb1%, lsb1%, msb0%, lsb0%

        OUT &H713, msb1%        'Output to D/A 1
        OUT &H712, lsb1%
        OUT &H711, msb0%        'Output to D/A 0
        OUT &H710, lsb0%

        'INPUT a$
WEND

'Get phase shifter calibration data
CALL arload(new$, "c:\quick500\paul\pscalq.dat")
```

```
CALL arstatus(new$, dep!, wid%, lp!, lab$)
CALL argetf(new$, 3!, dep! - 2!, 1, "", psbuf!(), -1)
CALL ardel(new$)

'Open ASCII file
OPEN "c:\quick500\paul\dummy.dat" FOR OUTPUT AS #1

'Since the A/Ds can only handle 10v maximum, a voltage divider had to
'be used to sample the voltage on channel 0. Hence the actual voltage
'on channel 0 is is the measured voltage multiplied by the inverse
'of the voltage divider (conversion factor)
cv! = 2.9988

FOR i! = 1! TO dep! - 4!
        newbuf!(i!) = psbuf!(i!) * cv!
        PRINT #1, i!, newbuf!(i!)
NEXT i!

'Close ASCII file
CLOSE #1

CALL armake("avbufq!", 1!, -1, "amm20")
CALL arputf("avbufq!", 1!, dep! - 4!, -1, "amm20", newbuf!(), 1)
CALL arlabel("avbufq!", "Voltage (mV) vs Phase (Degees)")
CALL arsave("avbufq!", "c:\quick500\paul\sample0q.dat")
CALL ardel("avbufq!")

'Get phase shifter calibration data
CALL arload(new$, "c:\quick500\paul\sample0q.dat")
CALL arstatus(new$, dep!, wid%, lp!, lab$)
CALL argetf(new$, 1!, dep!, 1, "", psbuf!(), -1)
CALL ardel(new$)

'Open ASCII file
OPEN "c:\quick500\paul\dummy2.dat" FOR OUTPUT AS #2

FOR i! = 1 TO dep! - 1!
       PRINT #2, i!, INT(psbuf!(i!))
NEXT i!

'Close ASCII file
CLOSE #2
```

# REFERENCES


Beheim, G. and Fritsch, K. Remote displacement measurements using a laser diode. *Electronics Letters*, 1985, *21*, 93-94.

Bendat, J.S. and Piersol, A.G. *Engineering Applications of Correlation and Spectral Analysis*. New York: John Wiley & Sons, 1980.

Betzig, E., Lewis, A., Harootunian, A., Isaacson, M. and Kratschmer, E. Near-field scanning optical microscopy (NSOM) - Development and biophysical applications. *Biophysical Journal*, 1986, *49*, 269-279.

Bobroff, N. Residual errors in laser interferometry from air turbulence and nonlinearity. *Applied Optics*, 1987, *26*, 2676-2682.

Born, M. and Wolf, E. *Principles of Optics*. Oxford: Permagon Press, 1980.

Bowick, C. *RF Circuit Design*. Indianapolis: Howard W. Sams & Co., 1986.

DeLange, O.E. Optical heterodyne detection. *IEEE Spectrum*, October 1968, 77-85.

Economou, G., Youngquist, R.C. and Davies, D.E.N. Limitations and noise in interferometric systems using frequency ramped single-mode diode lasers. *Journal of Lightwave Technology*, 1986, *LT-4*, 1601-1608.

Ellis, G.W. Piezoelectric micromanipulators: Electrically operated micro-manipulators add automatic high speed movement to normal manual control. *Science*, 1962, *138*, 84-91.

Estler, W.T. High accuracy displacement interferometry in air. *Applied Optics*, 1985, *24*, 808-815.

Eykhoff, P. *System Identification: Parameter and State Estimation*. London: John Wiley & Sons, 1974.

Eynon, J.U., Kolb, W.P. and Ramsay, I.A. Manufacturing low-noise HeNe lasers. *SPIE: Advances in Laser Engineering*, 1977, *122*, 174-178.

Foreman, J.W. Optical path length difference effects in photomixing with multimode gas laser radiation. *Applied Optics*, 1967, *6*, 821-826.

Frantz, L.M., Sawchuk, A.A. and Ohe, W.V.D. Optical phase measurement in real time. *Applied Optics*, 1979, *18*, 3301-3306.

Gasvik, K.J. *Optical Metrology*. Chichester: John Wiley & Sons, 1987.

Hariharan, P. Interferometric metrology: Current trends and future prospects. *SPIE: Interferometric Metrology*, 1987, *816*, 2-18.

Haykin, S. *Communication Systems*. New-York: John Wiley & Sons, 1983.

Hecht, E. *Optics* Readding: Addison-Wesley Publishing Company, 1987.

Higuchi, T., Yamagata, Y., Furutami, K. and Kudoh, K. Precise positioning mechanism utilizing rapid deformation of piezoelectric elements. *Proceedings: IEEE Micro Electro Mechanical Systems*, 1990, 222-226

Hollis, R.L., Salcudean, S. and Abraham, D W. Toward a tele-nanorobotic manipulation system with atomic scale force feedback and motion resolution. *Proceedings: IEEE Micro Electro Mechanical Systems*, 1990, 115-119.

Horowitz, P. and Hill, W. *The Art of Electronics*. Cambridge: Cambridge University Press, 1989.

Hunter, I.W. and Kearney, R.E. NEXUS: A Computer language for physiological systems and signal analysis. *Computers in Medicine and Biology*, 1984, *14*, 385-401.

Hunter, I.W., Lafontaine, S., Nielsen, P.M.F., Hunter, P.J. and Hollerbach, J.M. Manipulation and dynamic mechanical testing of microscopic objects using a tele-micro-robot system. *IEEE Control Systems Magazine*, 1990, *10*, 3-9.

Jacobs, S.F., Shough, D. and Connors, C. Thermal expansion uniformity of materials for large telescope mirrors. *Applied Optics*, 1984, *23*, 4237-4244.

Kikuta, H., Iwata, K. and Nagata, R. Distance measurement by the wavelength shift of laser light. *Applied Optics*, 1986, *25*, 2976-2980.

Kubota, T., Nara, M. and Yoshino, T. Interferometer for measuring displacement and distance. *Optics Letters*, 1987, *12*, 310-312.

Martel, S., Lafontaine, S. and Hunter, I.W. A parallel processing system for intensive I/O. *Proceedings: Canadian Conference on Electrical and Computer Engineering*, 1990.

Massie, N.A. Digital heterodyne interferometry. *SPIE: Interferometric Metrology*, 1987, *816*, 40-48.

Masry,, E. and Cambanis, S. Consistent estimation of continuous-time signals from nonlinear transformation of noisy samples. *IEEE Transactions on Information Theory*, 1981, *IT-27*, 84-96.

Melles-Griot. *Optics Guide 4*. 1988

Microsoft Corp. *Programming in Basic (Version 4.5)*. 1988.

Microsoft Corp. *Learning to Use Microsoft Basic (Version 4.5)*. 1988.

Royer, D., Dieulesaint, E. and Martin, Y. Improved version of a polarized beam heterodyne interferometer. *IEEE 1985 Ultrasonics Symposium*, 432-435.

Smythe, R.A., Soobitsky, J.A. and Truax, B.E. Recent advances in interferometry at Zygo. *SPIE: Interferometric Metrology*, 1987, *816*, 95-105.

Steinmetz, C., Burgoon, R. and Herris, J. Accuracy analysis and improvements to the Hewlett-Packard laser interferometer system. *SPIE: Interferometric Metrology*, 1987, *816*, 79-94.

Stumpf, K.D. Real-time interferometer. *Optical Engineering*, 1979, *18*, 648-653.

Sutton, C.M. Non-linearity in length measurement using heterodyne laser Michelson interferometry. *Journal of Physics, E.Scientific Instrumentation*, 1987, *20*, 1290-1292.

Timmermans, C.J., Schellekens, P.H.J. and Schram, D.C. A phase quadrature feedback interferometer using a two mode He-Ne laser. *Journal of Physics, E:Scientific Instrumentation*, 1978, *11*, 1023-1026.

Tanaka, M. and Nakayama, K. A new optical interferometer for absolute measurement of linear displacement in the subnanometer range. *Japanese Journal of Applied Physics*, 1983, *22*, 233-235.

Tanaka, M., Yamagami, T. and Nakayama, K. Linear interpolation of periodic error in a heterodyne laser interferometer at subnanometer levels. *IEEE Transactions on Instrumentation and Measurement*, 1989, *38*, 552-554.

Waksberg, A.L. Signal processing systems for low frequency hydrophones. *MPBT Internal Report No. 1SR79-00093*, 1981.

Wagner, J.W. and Spicer, J.B. Theoretical noise-limited sensitivity of classical interferometry. *Journal of the Optical Society of America*, 1987, *4*, 1316-1326.

Weast, R.C., Astle, M.J. and Beyer W.H. *CRC Handbook of Chemistry and Physics*. Boca Raton: CRC Press Inc., 1984.

Webb, P.P., McIntyre, R.J. and Conradi, J. Properties of avalanche photodiodes. *RCA Review*, 1974, *35*, 234-278.

Wolf, E. *Progress in Optics XXIV*. Amsterdam: North-Holland, 1987.

Yang, K.H., Chen, L. and Zhang, S.Y. Laser interferometer using a dual interference method. *Electronics Letters*, 1987, *23*, 699-700.

Zhu, L.Y., Hallamasek, K.F. and Bogy, D.B. Measurement of head/disk spacing with a laser interferometer. *IEEE Transaction on Magnetics*, 1988, *24*, 2739-2741.